Rapid spatio-temporal variations in rift structure during development of the Corinth Rift, central Greece

Casey W. Nixon*[,1,3], Lisa C. McNeill[1], Jonathan M. Bull[1], Rebecca E. Bell[2], Robert L. Gawthorpe[3], Timothy J. Henstock[1], Dimitris Christodoulou[4], Mary Ford[5], Brian Taylor[6], Dimitris Sakellariou[7], George Ferentinos[4], George Papatheodorou[4], Mike R. Leeder[8], Richard E.Ll. Collier[9], Andrew M. Goodliffe[10], Maria Sachpazi[11], Haralambos Kranis[12]

[1]University of Southampton; [2]Imperial College London; [3]University of Bergen; [4]University of Patras; [5]CRPG-CNRS, University of Nancy; [6]University of Hawai'i; [7]Hellenic Centre for Marine Research; [8]University of East Anglia; [9]University of Leeds; [10]University of Alabama; [11]National Observatory of Athens; [12]National and Kapodistrian University of Athens

[*]**Corresponding Author Email and Address:**

Casey.Nixon@uib.no

Department of Earth Science, University of Bergen, Allegatn 41, 5020 Bergen, Norway

Key Points:

1. Offshore Corinth Rift evolution is investigated at high spatial and temporal resolution
2. Rift migration and localization of deformation are significant within the Corinth Rift
3. Changes in rift geometry and linkage of major rift faults occur at rapid 100 kyr timescales

Abstract

The Corinth Rift, central Greece, enables analysis of early rift development as it is young (<5 Ma), highly active and its full history is recorded at high-resolution by sedimentary systems. A complete compilation of marine geophysical data, complemented by onshore data, is used to develop a high-resolution chronostratigraphy and detailed fault history for the offshore Corinth Rift, integrating interpretations and reconciling previous discrepancies.
Rift migration and localization of deformation have been significant within the rift since inception. Over the last ca. 2 Myr the rift transitioned from a spatially complex rift to a uniform asymmetric rift, but this transition did not occur synchronously along-strike. Isochore maps at ca.100 kyr intervals illustrate a change in fault polarity within the short interval ca.620-340 ka, characterized by progressive transfer of activity from major S-dipping faults to N-dipping faults and southwards migration of discrete depocentres at ~30 m/kyr. Since ca.340 ka there has been localization and linkage of the dominant N-dipping border fault system along the southern rift margin, demonstrated by lateral growth of discrete depocentres at ~40 m/kyr. A single central depocentre formed by ca.130 ka, indicating full fault linkage. These results indicate that rift localization is progressive (not instantaneous) and can be synchronous once a rift border fault system is established. This study illustrates that development processes within young rifts occur at 100 kyr timescales, including rapid changes in rift symmetry, and growth and linkage of major rift faults.

1. Introduction

Over the past 20 years, numerous studies of syn-rift deformation have furthered our knowledge of fault and rift evolution, e.g. North Sea [*Fossen and Hesthammer*, 1998; *Cowie et al.*, 2005; *Bell et al.*, 2014], Gulf of Corinth rift [e.g.*Taylor et al.,* 2011; *Ford et al.*, 2013], East African Rift [*Hayward and Ebinger*, 1996], Rio Grande Rift [*Leeder and Mack*, 2009], Gulf of Suez [*Gawthorpe et al.*, 2003], Gulf of California [*Aragón-Arreola et al.*, 2005]. Studies of these evolving and mature rifts have recognized progressive strain localization as an important process in rift evolution on a variety of temporal and spatial scales. It is commonly thought that rifts develop an initially broad zone of complex deformation that becomes localized onto a smaller number of discrete and increasingly large faults [*Walsh et al.*, 2001; *Cowie et al.*, 2005] while sedimentation becomes focused into fewer, larger depocentres [*Gawthorpe and Leeder*, 2000; *Gawthorpe et al.*, 2003; *Cowie et al.*, 2007]. Furthermore, it has been shown that active faulting and strain migrate towards the rift axis with increasing extension, resulting in rift narrowing [*Gawthorpe et al.*, 2003; *Cowie et al.*, 2005]. Localization of deformation has also been predicted by both physical [e.g. *Ackermann et al.*, 2001; *Mansfield and Cartwright*, 2001] and numerical models [e.g. *Gupta et al.*, 1998; *Behn et al.*, 2002; *Huismans and Beaumont*, 2007].

Models of rift evolution are typically based on mature rifts and passive margins, where the first few Myr of rift history are unresolved. Most studies have only achieved rift-scale temporal resolutions of the order of >1 Myr due to reliance on field observations [e.g. Gulf of Suez; *Gawthorpe et al*., 2003] or deep offshore basins [e.g. North Sea; *Cowie et al.,* 2005]. Some studies have investigated the evolution of individual fault systems at finer spatial and temporal scale (10’s kyr), however, these studies have been restricted to recent activity only or are not at rift scale [e.g. *Morley et al.,* 2000; *Hemelsdaël and Ford*, 2014; *Nixon et al.*, 2014]. Therefore, details of variations in structural style, strain distribution and strain rate at high resolution (temporal resolution of 10^4-10^6 yrs and spatial resolution of 1-10’s km) at whole rift scale are rarely resolved.

The Corinth Rift (Fig. 1) initiated < 5 Ma [*Ori*, 1989] and is one of the most rapidly extending [10-16 mm/yr; *Bernard et al.*, 2006; *Clarke et al.*, 1998; *Briole et al.*, 2000] active rift systems on Earth today. The rift itself is significantly smaller (~100 km x ~40 km) than other rifts (e.g. East African Rift; Basin and Range) and therefore can be investigated in its entirety at high resolution. The rift has a simple history of N-S extension [*McKenzie*, 1972; *Roberts and Jackson*, 1991] and has not been magmatically overprinted. Hence, this rift is an ideal natural laboratory for investigating the early development of marine/lacustrine rift basins and rifted margins.

The Corinth Rift has been studied extensively both onshore [e.g. *Gawthorpe et al.*, 1994; *Leeder et al.*, 2002, 2012; *Roberts et al.*, 2009; *Ford et al.*, 2013] and offshore [e.g. *Stefatos et al.,* 2002; *Sachpazi et al.,* 2003; *Leeder et al.*, 2005; *McNeill et al.,* 2005; *Lykousis et al.*, 2007; *Sakellariou et al.*, 2007; *Bell et al.*, 2008, 2009, 2011; *Taylor et al.*, 2011; *Charalampakis et al.*, 2014; *Beckers et al.*, 2015] to extract syn-rift sedimentation, fault and rift architecture, and to quantify extension. However, the existing marine seismic datasets have never been fully integrated, resulting in contrasting interpretations of the rift structure, the absence of a uniform stratigraphic framework for the offshore rift, and similar but inconsistent chronostratigraphic models [e.g. *Sachpazi et al.*, 2003; *Leeder et al.*, 2005; *Sakellariou et al.*, 2007; *Bell et al.*, 2008, 2009; *Taylor et al.*, 2011].

This paper integrates all available offshore Corinth Rift seismic reflection data (summarized in Fig. 2), producing a dense network that is used to develop a uniform syn-rift stratigraphic and chronostratigraphic framework for the past ca. 1-2 Myr. This framework allows us to unravel the structural development of the Corinth Rift at higher temporal resolutions than previously achieved here or at any other continental rift. We focus on quantifying variations in the distribution of the syn-rift sediments through time, illustrating the across- and along-strike development of the offshore rift structure, and constraining the timeframes of switches in fault polarity and fault/depocentre linkage and localization. By quantifying the magnitude, rate and timing of early rift deformation at unprecedented spatial resolutions and on timescales <<1 Myr, we are able to address the following key questions: How does rift geometry evolve and on what timescale? Is strain localization an abrupt or gradual process? And does it occur synchronously along a rift?

2. Geological background and stratigraphy of the Corinth Rift

The Corinth Rift forms a high strain band of N-S extension across central Greece that has been active since the late Pliocene [*Skourlis and Doutsos*, 2003; *Leeder et al.*, 2008; *Ford et al.*, 2013; Fig. 1], with the modern active rift axis (offshore Gulf of Corinth) initiating ca. 2 Ma [e.g. *McNeill et al.*, 2005; *Bell et al.*, 2008, 2009; *Leeder et al.*, 2008]. Geodynamic models for the formation of the rift include extension associated with roll-back of the subducting African

Plate [*McKenzie*, 1978; *Doutsos et al.*, 1988; *Jolivet et al.*, 1994], gravitational collapse of over-thickened crust [*Le Pourhiet et al.*, 2003] and the SW propagation of the dextral North Anatolian Fault [*Armijo et al.*, 1996, 1999]. Present day geodetic rates of extension across the rift range from <5 mm/yr in the east to >10-15 mm/yr in the west [*Davies et al.*, 1997; *Clarke et al.*, 1998; *Briole et al.*, 2000; *Avallone et al.*, 2004]. However, long-term deformation patterns and whole-crust extension estimates indicate greater amounts of extension [~11-21 km; *Bell et al.,* 2011] in the central rift and extension at lower rates in the western rift [0.6-4.8 mm/yr; *Ford et al.,* 2013] in the past, indicating potentially significant temporal variations in strain distribution within the rift [*Bell et al.*, 2011; *Ford et al.*, 2013].

The onshore syn-rift sediments of the western and central rift have been separated into three lithostratigraphic groups: A Lower Group characterized by alluvial to lacustrine sediments deposited in the late Pliocene (estimated between ca. 4 Ma to 2.5-1.8 Ma) during a time of distributed extension; a ca. 2.5-1.8 Ma to 0.7-0.45 Ma Middle Group dominated by lacustrine fan deltas that built during a period of rift deepening and northward migration; and a ca. 0.7-0.45 Ma to present Upper Group characterized by alternating marine and lacustrine sediments [e.g. *Ori*, 1989; *Gawthorpe et al.*, 1994; *Rohais et al.*, 2007; *Backert et al.*, 2010; *Leeder et al.*, 2012; *Ford et al.*, 2013]. Up to ~2.5 km of syn-rift sediments have accumulated in the offshore Gulf of Corinth. These comprise a deeper sequence (defined here as Seismic Unit 1, SU1) that varies considerably in thickness and largely lacks continuous coherent reflections and by a sequence (defined here as Seismic Unit 2, SU2) that is well stratified, consisting of laterally continuous packages of reflections [*Sachpazi et al.*, 2003;

Lykousis et al., 2007; *Bell et al.*, 2008, 2009; *Taylor et al.*, 2011] separated from SU1 by an unconformity. Analyses of sediment cores indicate alternating marine and lacustrine conditions in recent times, caused by basin isolation during glacial lowstands by the Rion-Antirion sill in the west [e.g. Perissoratis et al., 2000]. Analysing seismic stratigraphy, previous studies have interpreted marine and lacustrine packages within SU2, correlating them with the Quaternary sea level, specifically 100 kyr glacio-eustatic cycles [different results summarized in Table 1; *Sachpazi et al.*, 2003; *Moretti et al.*, 2004; *Leeder et al.*, 2005; *Lykousis et al.*, 2007; *Sakellariou et al.*, 2007; *Bell et al.*, 2008, 2009; *Taylor et al.*, 2011]. Thus the existing tectono-stratigraphic framework for the offshore Corinth Rift needs to be reconciled in order to accurately analyse sediment flux and fault activity history around the rift.

3. Methodology

Seismic reflection data

All available 2D seismic reflection data from the offshore Corinth rift were compiled and integrated, including high resolution seismic, multi-channel seismic and scanned analogue data that cover a range of frequencies, totalling >5000 km of seismic profiles (summarized in Fig. 2). Primarily, four seismic surveys were used for correlating faults and for the basin wide chronostratigraphic interpretation:

1) *R/V Maurice Ewing 2001* - MCS data penetrating the complete syn-rift sequence to basement throughout the Gulf, previously published by *Zelt et al.* [2004] and *Taylor et al*. [2011].

2) *M.V. Vasilios 2003* - High resolution MCS data penetrating all or part of the syn-rift sequence in the western Gulf of Corinth, previously published by *McNeill et al.* [2005], *Bell et al*. [2008, 2009].
3) *R/V AEGAEO* - High resolution single channel data penetrating all or part of the syn-rift sequence throughout the Gulf previously published, in part, by *Lykousis et al*. [2007] and *Sakellariou et al*. [2007].
4) *M.V. Vasilios 1996* - High resolution single channel data in the Alkyonides Gulf previously published by *Collier et al*. [2000], *Leeder et al*. [2002, 2005], *Stefatos et al*. [2002] and *Bell et al*. [2009].

Local datasets including airgun profiles, single channel sparker profiles and sub-bottom profiles [e.g., *Stefatos et al*., 2002; *Charalampakis et al*., 2015] were used to confirm correlation and location of faults, in particular along the southern margin. Details of each seismic reflection survey can be found in the relevant publications listed in Figure 2.

Stratigraphic interpretation

The dense network of seismic profiles allows us to accurately trace key seismic reflections within Seismic Unit 1 (SU1) and Seismic Unit 2 (SU2) throughout the offshore rift. We focus on areas east of Aigion where deep penetrating seismic data are present (Figs. 1 and 2). The seismic stratigraphy is interpreted using the same techniques of previous studies (Table 1), specifically distinguishing marine and lacustrine packages within SU2:

1. Sedimentary structures and geometries: prograding clinoforms, truncation and onlap on the upper slopes and shelf regions of the offshore rift. Following previous studies [e.g. *Leeder et al*., 2005; *McNeill*

et al., 2005; *Bell et al.,* 2008, 2009], we interpret clinoforms as forming in lowstand, lacustrine conditions with onlapping marine sediments marking transgression.

2. Seismic character – In the main basin, changes in amplitude and frequency were used to divide the stratigraphy [methods of *Sachpazi et al*., 2003; *Lykousis et al*., 2007; *Bell et al*., 2008, 2009; *Taylor et al*., 2011), calibrated with Marion Dufresne long piston cores [*Moretti et al*., 2004] sampling the last ~ 20-25 ka [see *Bell et al*., 2008]. We use this method to identify lacustrine and marine packages within the seismic stratigraphy by picking the base horizon of higher amplitude packages, interpreted as the onset of marine sedimentation (e.g. Fig. 3).

The alternating marine and lacustrine packages within SU2 can be correlated with ca. 100 kyr glacio-eustatic cycles [sea level curve of *Bintanga and van der Waal*, 2008], providing age estimates for each stratigraphic horizon for the past ca. 700 kyr. Proposed ocean drilling of the section will allow us to ultimately test the accuracy of this framework [*McNeill et al.,* 2014].

Sediment distribution analysis for fault activity

The SU2 stratigraphic horizons provide a high-resolution framework (1 km x 1 km; 100 kyr) to generate isochore maps and along-strike profiles of maximum sediment thickness. Sediment thicknesses are calculated using a linear velocity model [based on: tomography data, *Zelt et al*., 2004; pre-stacked depth migration, *Clement,* 2000; semblance plots, *Bell et al*., 2008; and geophysical core logs, *Collier et al.,* 2000 and *Moretti et al*., 2004] that increases at 1.5 km s^{-1} s^{-1} from the seafloor where the velocity is 1.55 km s^{-1} *[Moretti et al*., 2004]. Sediments were decompacted using a porosity-depth relationship for calcareous sediments [Goldhammer, 1997]. Patterns in syn-rift sediment thickness were used to understand the links between fault and depocentre locations following an assessment of the contribution of fluvial sediment input to sediment thickness. Fault polygon maps are used to illustrate the cumulative heave on faults for key time intervals. The length and width of the fault polygons are generated using hanging wall and footwall cut-off points and identifying realistic along-strike fault heave patterns. The fault polygons were superimposed onto the isochore maps allowing us to assess depocentre development and fault activity.

4. Uniform stratigraphic framework for the offshore Corinth Rift

The two seismic units (SU1 and SU2) are separated by a basin-wide unconformity (horizon U), which marks an abrupt change in seismic character between the two units [e.g. Fig. 3; *Sachpazi et al.*, 2003; *Bell et al.*, 2009; *Taylor et al.*, 2011]. SU1 is characterized by lower amplitude reflections that lack coherency (Fig. 3). In contrast, within SU2 we can clearly identify six high amplitude marine packages (package bases H1-H6) and low amplitude lacustrine packages, which we correlate with the last six ca. 100 kyr glacio-eustatic cycles (Fig. 3).

This chronostratigraphic interpretation is similar to that proposed by Sachpazi et al. (2003) but they do not recognise the most recent marine stage. Our interpretation matches Taylor et al. [2011] back to ca. 480 ka, however, prior to ca. 480 ka they compress sedimentation during the short lacustrine stage and surrounding marine stages of ca. 620-480 ka into one reflection (our H6, Fig. 3).

Taylor et al. [2011] correlates the thick low-amplitude unit above the unconformity with the ca. 680-620 ka lacustrine stage, and the unconformity with the ca. 710-680 ka marine stage. Instead we allow for a local expansion of sedimentation during the short ca. 560-530 ka lacustrine stage, and correlate the unconformity with the onset of the ca. 620-560 ka marine stage. Our model is preferred because: a) it maintains the correlation of high and low amplitude packages with marine and lacustrine conditions, respectively; and b) it avoids significant changes in sedimentation rate. The unconformity and base of SU2 is therefore ca. 620 ka (horizon U; Fig. 3).

SU2 can be directly correlated into the Lechaion Gulf, consistent with the interpretations of *Taylor et al.* [2011] and *Charalampakis et al.* [2014]. Horizons for the last ca. 240 kyr can also be correlated into the Alkyonides Gulf, matching well defined clinoform interpretations of *Leeder et al.* [2005] and consistent with Bell et al. [2009] (Table 1 and Fig. 4a). All SU2 horizons can be traced east to west along the whole Gulf of Corinth (Fig. 4b), and are laterally continuous and conformable with the exception of the western Gulf, where H4 truncates underlying sediments forming a second unconformity. This is the unconformity interpreted by *Bell et al.* [2008, 2009], previously misinterpreted as being correlative with the older unconformity in the thicker central basin sequence. Therefore, there are two unconformities in the western Gulf of Corinth: the basin-wide SU1-SU2 unconformity at ca. 620 ka; and a younger unconformity at ca. 340 ka local to the upper shelf and margins of the western Gulf of Corinth.

Our interpretation reconciles previous chronostratigraphic discrepancies (e.g. Table 1, Fig. 3d). Using the ca. 620 ka age of the basin-wide unconformity (U) and the thickness of SU2 and SU1, we estimate an age of ca. 1.5-2 Ma for the oldest sediments within the offshore rift using decompacted sedimentation rates of SU2, matching ages of Bell et al. [2009].

5. High resolution along-strike rift structure and fault network

In this section, we present and describe a new, highly detailed and more precise Corinth Rift fault map (Fig. 1) with fault activity history and differences in the development of rift geometry along the rift (Figs. 5, 6, Table 2). We divide the rift into five along-strike domains.

West Gulf of Corinth

The Trizonia Basin, west of Aigion (Fig. 1 and 5), is predominantly controlled by the Psathopyrgos, Trizonia and Aigion Faults [*Beckers et al.,* 2015]. East of Aigion, the southern margin is segmented into the active, en-echelon, N-dipping Aigion, Diakopto, West Eliki and East Eliki Faults (Fig. 5). Syn-rift sediments are mainly deposited in a narrow symmetrical graben primarily controlled by the S-dipping West Channel Fault to the north and the N-dipping Eliki Faults and currently inactive Pyrgaki-Mamoussia Faults to the south (Figs. 5 and 6a). The laterally constant thickness between key horizons (i.e., basement, U, H4 and H2; Fig. 6a) indicates approximately equal activity on the N- and S-bounding faults (Fig. 5) during deposition of SU1 and SU2. In the footwall of the West Channel Fault, the syn-rift sequence is significantly thinner, with only SU2 present and horizon H4 becomes unconformable (Fig. 6a). The South and North Eratini Faults, uplifting the northern horst block that forms the southern boundary of the Eratini sub-basin, are interpreted as active since deposition of

SU2 (ca. 620 ka) [as per *McNeill et al*., 2005; *Bell et al*., 2008]. The locus of rift-related subsidence stepped northwards in this part of the rift at ca. 620 ka and, depending on the relative timing of the primary southern margin faults (Eliki and Derveni) and the Eratini Faults, the rift may have also widened. See also discussions by *Bell et al*. [2008], *Ford et al*. [2013], *Taylor et al*. [2011].

Central-West Gulf of Corinth

Along the northern margin a single large S-dipping fault with a length of ~40 km has been named the East Channel or the Galixidi Fault [*Bell et al*., 2008, 2009; *Taylor et al.,* 2011], however, our denser seismic network shows that this fault is composed of multiple linked and unlinked segments. The segments that are fully linked at basement depth form what we now call the Galaxidi Fault (Fig. 5). The remaining unlinked western fault segment ~8 km in length, situated between the West Channel Fault and the Galaxidi Fault, is now referred to as the East Channel Fault (Fig. 5).

The syn-rift sediments deposited between the Derveni and Galaxidi Faults form an overall symmetrical graben, but with a switch in fault dominance from S-dipping to N-dipping faults over time [Fig. 6b; *Sachpazi et al*., 2003; *Bell et al.,* 2009; *Taylor et al.,* 2011]. Our new integrated data allow the extraction of details of this transition. The Galaxidi Fault was dominant during SU1 (Fig. 6b; Table 2), but ca. 620-340 ka a more symmetrical package of syn-rift sediments was deposited indicating a discrete transition period with equal N- and S-dipping fault activity (Fig. 6b). Shortly after ca. 340 kyr (horizon H4), the Galaxidi Fault became buried and inactive, coinciding with the formation of a S-thickening half graben controlled by the N-dipping Derveni Fault. The sediments of SU2 are deformed by numerous small S-dipping faults between the Galaxidi and Derveni Faults (Fig. 6b), often associated with an anticlinal structure that forms around a pivot point, potentially a damage zone related to the polarity reversal and transfer of strain.

Central-East Gulf of Corinth

The Derveni Fault is hard linked to the Lykoporia Fault, forming a significant N-dipping fault, ~40 km in length, bounding the southern margin of the central basin (Figs. 5, 6b). The now inactive West Xylokastro Fault (onshore) and active East Xylokastro Fault (offshore) both sit in the footwall of the Lykoporia Fault [Fig. 5; *Bell et al*., 2009]. The northern margin is characterised by numerous smaller and less significant S-dipping faults, including some previously unmapped faults on the shelf/slope that unusually trend NE-SW, with the main depocentre bound by the S-dipping West and East Antikyra Faults (Figs. 5, 6c). A thin package of SU1 sediments (~300 ms TWTT, <400 m thick) are deposited in a narrow symmetrical graben in this Domain (Fig. 6c). Since ca. 620 ka (SU2), the N-dipping Lykoporia and East Xylokastro Faults have generated a half-graben (Fig. 6c), with the S-dipping Antikyra Faults (WAN, EAN) on the northern margin less active. The minor S-dipping faults in the footwall of the WAN and EAN, appear to have activated during SU2 deposition, suggesting the northern rift margin has stepped north during SU2.

East Gulf of Corinth

In the main basin during SU1 deposition, multiple basement horst structures are uplifted by S-dipping faults creating small N-thickening half-graben [see also *Bell et al*., 2009]. The horsts became buried and inactive by ca. 340 ka (Fig. 6d). Along the southern margin of this basin, the N-dipping North Kiato and Perachora Faults, ~12 km in length,form a dextral en echelon fault array with the East Xylokastro Fault which is probably linked at depth. In contrast to previous studies that interpret the Perachora Fault as a NE-trending fault [e.g. *Stefatos et al*., 2002; *Lykousis et al.,* 2007; *Bell et al*., 2009; *Taylor et al*., 2011; *Charalampakis et al*., 2014], we have identified its continuation closer to the Perachora Peninsula. This interpretation gives the Perachora fault an ENE-trend, more consistent with adjacent faults. SU2 sediments thicken and tilt to the south, forming an asymmetrical graben controlled by the N-dipping Perachora Fault (Fig. 6d). The rift zone stepped north around ca. 620 ka with upper SU1 and lower SU2 sediments draping the northern rift margin up to the S-dipping Vroma Fault (Figs. 5, 6d).

The Heraion Ridge, bound by the Perachora Fault to the north and the Heraion and Lechaion Faults to the south [Figs. 5 and 6d; *Charalampakis et al*., 2014], separates the Gulf of Corinth from the Lechaion Gulf. This ridge continues onshore at the Perachora Peninsula. In the Lechaion Gulf, SU1 and SU2 thicken in the hanging wall of the S-dipping Heraion and Lechaion Faults, indicating their activity, and thin on top of the Heraion Ridge (Fig. 6d) [see also *Charalampakis et al*., 2014].

Alkyonides Gulf

The Alkyonides Gulf is separated from the Gulf of Corinth by the fault-bounded horst of the Alkyonides Islands (Fig. 5). The southern Alkyonides margin is controlled by the N-dipping Strava, West Alkyonides and East Alkyonides Faults [*Leeder et al*., 2002; 2005; *Sakellariou et al*., 2007]. The NE-SW trending Livadostras Fault controls the northern margin and the West and East Domvrena Faults form a minor sub-basin to the north of the Alkyonides Islands [see also *Sakellariou et al*., 2007; *Leeder et al.*, 2002; *Bell et al*., 2009]. The Alkyonides Gulf forms an apparently simple S-tilting half-graben structure dominated by N-dipping faults (Figs. 5, 6e) [*Sakellariou et al*., 2007; *Leeder et al*., 2002; *Bell et al*., 2009]. However, prior to ca. 340 ka (below horizon H4; Fig. 6e), uniform sediment thickness indicates equal activity on both S-dipping and N-dipping faults [see also *Sakellariou et al*., 2007]. Since ca. 340 ka, the N- to NW-dipping West and East Alkyonides faults have dominated, generating the half graben (Fig. 6e).

Summary of along-strike rift structure

Most along-strike rift domains show an evolution towards a simple south-thickening half-graben controlled by N-dipping faults (Table 2; Fig. 6). The western Gulf of Corinth (Aigion to Diakopto) is the exception, with N- and S-dipping active faults forming a complex but symmetrical graben [e.g. *McNeill et al*., 2005; *Bell et al*., 2008]. The ca. 620 ka unconformity (U) marks a major period of change in dominant fault polarity and rift symmetry with a transition period that lasted ca. 300 kyr (ca. 620-340 ka). At the end of this transition period, H4 (ca. 340ka) is unconformable in the western Gulf and major S-dipping faults became inactive throughout the rift (Fig. 6). After ca. 620 ka, the northern rift margin stepped to the north throughout most of the Gulf of Corinth with minor S-dipping faults activating north of the previous northern rift margin (Figure 7). This timing of increased strain distribution coincides with the switch in fault polarity at ca. 620-340 ka.

6. Depocentre development and fault linkage history - refined and improved resolution

Primary stages of rift depocentre development

We have generated isochore maps for each syn-rift interval, building on the work of *Bell et al*. [2009] and *Taylor et al*. [2011], with significantly increased accuracy both temporally and spatially (Figs. 7, 8, 9). Basement depth (Fig. 5) indicates a single depocentre ~70 km in length (between Diakopto and Perachora) in the Central Domains (up to 3000 ms TWTT below sea level) with much shallower depths in the Alkyonides and West Domains (~1000 ms TWTT below sea level). The new isochore maps indicate (Fig. 7) that before ca. 620 ka (SU1; Fig. 7a) syn-rift sediments were deposited in two separate depocentres. One in the hanging wall of the S-dipping Galaxidi Fault (Central-West Domain); another bound by the N-dipping North Kiato Fault and buried S-dipping faults (East Domain). After ca. 620 ka (SU2; Fig. 7b) these depocentres became linked to form a single large depocentre, ~50km in length, in the hanging walls of the N-dipping Derveni, Lykoporia and East Xylokastro Faults. Depocentre thickness is primarily influenced by sediment supply and creation of of accommodation space. As discussed in the next section, sediment supply does not appear to play a significant role, thus we can use thickness variations as a proxy for fault development.

Syn-rift sediment distribution indicates a major shift in rift structure from a complex rift zone controlled by both N- and S-dipping faults (Fig. 7a), to a uniform asymmetric rift controlled by N-dipping faults (Fig. 7b). High-resolution 100 kyr interval isochore maps (Figs. 8 and 9) highlight this establishment of an asymmetric rift over two phases: **1)** a change in fault polarity over a discrete time interval (ca. 100-300 kyr) between ca. 620-340 ka; and **2)** linking of depocentres since ca. 340 ka.

The nature of the switch in fault polarity

Between ca. 620-340 ka (Fig. 8), discrete depocentres were formed by both N-dipping and S-dipping faults (i.e. the Derveni and Lykoporia Faults, and Galaxidi Fault, respectively). Initially (ca. 620-530 ka) the depocentres were dominated by major S-dipping faults, for example the Galaxidi Fault controlled two discrete depocentres >200 ms TWTT (>250 m) thick in the north (Fig. 8a). The depocentres progressively migrated southward during ca. 530-420 ka with central maximum sediment accumulation (Fig. 8b) and maximum sedimentation finally reached the southern rift margin and hanging walls of major N-dipping faults (e.g. East Eliki and Derveni Faults) during ca. 420-340 kyr. (Fig. 8c). This final stage (ca. 420-340 ka) occurred along the entire length of the Gulf of Corinth southern margin (i.e. East Eliki, Derveni, Lykoporia, East Xylokastro Faults; Fig. 8c). The East Alkyonides Fault also began to dominate sediment deposition in the Alkyonides Gulf during this time interval (Fig. 8c). Thus N-dipping faults have dominated subsidence and deposition throughout the active rift zone, creating a uniform asymmetric offshore rift since ca. 340 ka. The depocentres migrated southwards at a rate of ~30 m/kyr suggesting a progressive strain transfer.

Depocentre growth and linkage since ca. 340 ka

Since ca. 340 ka, discrete depocentres in the hanging walls of the N-dipping East Eliki, Derveni, Lykoporia and East Xylokastro Faults have started to grow and link (Fig. 9a). Major S-dipping faults have become buried and inactive and in some cases propagated upward as smaller fault segments (e.g., Galixidi Fault; Fig. 9a), no longer influencing depocentre development.

Between ca. 340-240 ka (Fig. 9a), a number of small discrete depocentres, ~4 km in length with ~200 ms TWTT (~250 m) sediment thickness, formed in the hanging walls of the East Xylokastro, Lykoporia and Derveni Faults and between the now linked Derveni and East Eliki Faults. These discrete depocentres grew in size, increasing in length at a rate of ~40 m/kyr to form three partially linked depocentres, ~8-12 km in length with >200 ms TWTT (>250 m) sediment thickness, by ca. 240-130 ka (Fig. 9b). The Perachora Fault also generated a smaller depocentre in the eastern Gulf of Corinth during this time period.

The depocentres grew substantially from ca. 130 ka to present day (Fig. 9c), linking to form a major depocentre ~40 km in length with up to 400 ms TWTT (~400 m) of post-130 ka accumulated sediments. The depocentre offshore Akrata was smaller with relatively high subsidence offshore Lykoporia. Overall the most significant region of sediment accumulation shifted eastward, to offshore Xylokastro (Figs. 9c, 10). The Alkyonides Gulf depocentre (in the hanging wall of the West and East Alkyonides Faults) also increased in relative thickness. Therefore, since ca. 340 ka, depocentres along the southern margin of the offshore Corinth Rift have increased in size, thickness and degree of linkage, reflecting the localization of deformation and linkage of the major N-dipping fault system that bounds the southern margin.

Quantifying offshore sediment accumulation and depocentre development

The major spatial shifts in distribution of syn-rift sediments is further illustrated by along-strike profiles of maximum sediment thickness (Fig. 10). Depocentre development is influenced by a combination of hanging wall subsidence and sediment supply. Present day major river systems and associated deltas are evenly distributed along the Peleponesse coastline (Fig. 10). The positions of these river systems can be fault controlled [e.g. the Krathis River; *Hemelsdaël and Ford*, 2014] but their positions for the most part do not align with peaks in maximum sediment accumulation rate, which vary temporally and are often coincident with the centre of individual fault segments (Fig. 10d, e). Thus, sediment input does not appear to be the most important control on patterns of syn-rift sediment thickness. Instead sediment distribution appears to be predominantly fault-controlled and, with sufficient sedimentation rates, should be an accurate measure of the growth and activity of major basin bounding faults (e.g. Fig. 10) and basin subsidence.

From ca. 2-1.5 Ma to 620 ka (SU1), variations in the maximum unit thickness show peaks in sediment accumulation at ~625000 m and ~655000 m (UTM coordinates; Fig. 10b), coinciding with the two depocentres (Fig. 7a). However, maximum sediment thickness for SU2 (ca. 620 ka – present) is at ~640000 m (UTM coordinates; Fig. 10b), directly between the two peaks of SU1, illustrating the shift in sediment accumulation towards the centre of the rift due to depocentre linkage (Fig. 7b). The combined effect of these two phases produces a maximum total sediment thickness distribution with a flattened bell-curve shape (Fig. 7a) over the last 1.5-2 Myr.

Comparison of maximum sediment accumulation rates for different time intervals since ca. 620 ka (Fig. 10c,d) show that overall rates have been relatively constant, averaging 1-3 m/kyr and sufficient to record deformation despite an under-filled present day basin. However, within each ca. 100 kyr interval there are more localized peaks in maximum sediment accumulation rate, coincident with the depocentres in the major basin-bounding fault hanging walls (i.e. Fig. 10e).

The maximum sediment accumulation rate profiles combined with isochore maps (Figs. 8, 9) indicate that the overall shift in sediment distribution and depocentre development occurs gradually over the past 620 kyr. During ca. 620-340 ka, the peaks in maximum rate change from being quite irregular in size and distribution (i.e. ca 620-530 ka; Fig. 10c) to forming five consistent peaks that are evenly distributed and similar in size (i.e. ca. 420-340 ka; Fig. 10c), reflecting the change in fault polarity/rift symmetry (Fig. 8). Since ca. 340 ka there are a smaller number of peaks in the profiles of maximum sediment rate that eventually form a broad bell-curved profile with a central peak at

645000 m (UTM coordinates; Fig. 10d), representing the growth and linkage of the faults and depocentres (Fig. 9).

7. Summary of Corinth Rift evolution from inception ca. 4 Ma to present

The onshore stratigraphic model of Lower, Middle, and Upper groups [*Rohais et al*., 2007; *Ford et al*., 2013; *Leeder et al*., 2012], is widely used, but limited datable material means that there are no absolute ages for the boundaries between the groups and discrepancies exist between studies. Therefore, we use a range of ages for each group that encompass these age estimates (Table 3) and apply the broad chronology to the rest of the onshore rift.

Our proposed ages for seismic stratigraphic units SU1 (ca. 2-1.5 Ma to 0.6 Ma) and SU2 (ca. 0.6 Ma to present) chronologically correspond with the age estimates for the Middle Group (ca. 2.5-1.8 Ma to 0.7-0.45 Ma) and Upper Group (ca. 0.7-0.45 Ma to present), respectively [Table 3; *Rohais et al*., 2007; *Leeder et al.,* 2012; *Ford et al*., 2013]. Combined with new insights of offshore fault activity, and previously published onshore fault activity this correlation allows us to refine the general evolution of the Corinth Rift over the last ca. 4 Myr (Fig. 11).

Late Pliocene to Early Pleistocene (ca. 4 Ma to 2.5-1.8 Ma)

The earliest syn-rift sediments [ca. 4-3.6 Ma; *Rohais et al*., 2007], within the Lower Group, occurred onshore and were deposited in a rift with distributed faulting and significant inherited relief [*Collier and Jones*, 2003; *Ford et al.*, 2007, 2013; *Rohais et al.*, 2007]. The majority of the Lower Group sediments (Fig. 11a) were defined by: a series of N-dipping faults, including the Dhemesticha and Kalavryta Faults, and possibly a buried S-dipping fault in the western rift [*Ford et al*., 2013; Wood et al., 2015]; the Kellini Fault and the Koutsa Fault/Xylokastro Horst block in the central rift [*Leeder et al*., 2008, 2012]; and the Klenia Fault and Loutraki/Lechaion Faults in the eastern rift, which marked the northern margin of the Corinth-Nemea basin [*Collier and Dart*, 1991; *Charalampakis et al*., 2014]. Our age correlation suggests that the Lower Group sediments are minimal/absent offshore suggesting little or no deformation and associated subsidence there before ca. 2 Ma [*Bell et al*., 2009], however this cannot be confirmed without direct sampling. In the Alkyonides Gulf the onshore syn-rift sediments formed in the NW-SE trending Megara basin at this time [*Leeder et al*., 2008] and equivalent sediments are likely in the base of the eastern Alkyonides basin either fault bound or infilling pre-exisitng basement topography [*Sakellariou et al*., 2007].

Early Pleistocene to Late Pleistocene (ca. 2.5-1.8 Ma to ca. 0.6 Ma)

Deformation migrated northwards [*Leeder et al*., 2008; *Ford et al*., 2013] and became more focused onto individual N- and S-dipping faults during deposition of the Middle Group [*Ford et al.*, 2007; *Rohais et al.*, 2007; *Bell et al.*, 2009]. A major depocentre in the western rift was bound by the onshore Pyrgaki-Mamoussia Fault along the southern margin and controlled by the offshore

Galaxidi Fault [Fig. 11b; *Ford et al*., 2013]. In the central rift, our data indicate minimal sedimentation offshore Xylokastro at this time, likely due to the onshore Xylokastro Horst Block confining Gilbert fan delta deposits to the south [Fig. 11b; *Leeder et al*., 2012]. Deformation was apparently accommodated by a number of S-dipping faults, including the Heraion Fault, in the eastern rift [Fig. 11b; *Charalampakis et al*., 2014]. In the Megara basin, deformation ceased and transferred north-west to the Alkyonides Gulf between ca. 0.8-2.2 Ma with initiation of N- to NW-dipping faults on the southern margin of the Alkyonides Gulf [*Leeder et al*., 2008].

Late Quaternary (ca. 0.6 Ma to present)

The rift migrated further north with the majority of Upper Group sediments deposited in the modern offshore rift (Figs. 11 c and d). Major S-dipping faults (i.e. Galaxidi Fault) decreased in activity between ca. 620-340 ka and depocentres became focused along the southern margin (Fig. 11c). The western rift is an exception because of activation of the the N- and S-dipping Eratini Faults [*McNeill et al*. 2005; *Bell et al*., 2008, 2009], whereas deformation in the central rift became focused on the N-dipping Derveni, Lykoporia and Xylokastro Faults. The eastern rift was characterised by numerous horst blocks as the N-dipping Perachora Fault also became more active. Since ca. 340 kyr, the major N-dipping faults, such as the Eliki, Derveni, Lykoporia, Xylokastro and Perachora Faults, have increased in activity to control a single major depocentre along the southern margin of the Gulf of Corinth. In contrast, deformation of the northern margin is now taken up by numerous distributed S-dipping faults (Fig. 11d). In the Alkyonides Gulf, deformation has become focused on the N-dippng East Alkyonides Fault, and the Heraion Fault continues to control deposition in the Lechaion Gulf.

8. Discussion

This is one of the first studies of its kind to look at key rift evolutionary processes such as rift geometry evolution, depocentre development and fault linkage at such unprecedented resolutions (~100 kyr and ~1 km) across an entire rift, and can now be compared with different models of rift development and with more mature rift systems.

Rapid changes in fault polarity and rift symmetry

The development of asymmetry in a rift zone is relatively common, for example in much of the East African rift zone [*Ebinger and Scholz*, 2012]. Many studies have documented spatial variability in fault polarity and rift symmetry within rifts, including the Gulf of Suez [*Patton et al.*, 1994; *Bosworth et al.*, 2005], East Africa [*Rosendahl,* 1987; *Hayward and Ebinger*, 1996], the now inactive North Sea [*Cowie et al.*, 2000] as well as fully evolved passive margin settings [*Mohammed et al.,* 2016]. Models indicate that rift development should be spatially and temporally variable due to variations in fault timing and activity, with rifts developing from numerous isolated basins to a single laterally continuous half-graben [e.g. *Cowie et al*., 2000]. Such models show a consistent dominant fault polarity throughout rift development. However, our observations from the offshore Corinth Rift indicate a spatially complex rift zone with both N- and S-dipping faults dominating at different times, before forming a uniform asymmetric rift controlled by N-dipping faults (Figs, 7, 8 and 9).

For the first time we can constrain the rate of polarity and symmetry change within a rift and determine the discrete time interval for this process in parts of the rift. We show that this is a rapid but progressive (rather than instantaneous) process, taking place over a time interval as small as 300 kyr. The transition to a more simple asymmetric rift is characterized by a decrease in activity and death of major S-dipping faults as strain is transferred onto major N-dipping faults. For example, in the Central-West Domain of the rift, strain transfers from the Galaxidi Fault to the Derveni Fault (Fig.8b, 12a-12b). The decrease in activity of major S-dipping faults results in the local unconformity observed within their footwall blocks in the western rift at ca. 340 kyr (e.g. Fig. 6a). An accommodation zone of numerous conjugate minor faults forms around a pivot point in the rift axis at this time of polarity/symmetry change (Fig. 6b). Similar conjugate zones of distributed deformation have been documented and are thought to show interaction between domains of differing fault polarity [e.g. *Nelson et al.,* 1992; *Fossen and Hesthammer*, 1998; *Kornsawan and Morley,* 2002; *Schlische and Withjack*, 2009; *Nixon et al.,* 2011]. The polarity change across the rift results in north to south migration of depocentres (Fig. 8, 12), towards the southern margin and the hanging walls of the major rift border faults (Figs. 11, 12b).

Although asymmetry within the rift develops over a particular period, the resolution of our dataset allows us to determine that asymmetry does not develop synchronously along-strike (Fig. 6; Table 2). Major N-dipping faults have dominated in the Central-East and East Domains since ca. 620 ka forming

S-thickening half-graben (Figs. 6c and 6d; Table 2), whereas deformation in the Central-West Domain and the Alkyonides was not dominated by N-dipping faults until ca. 340 ka (Fig. 6b and 6e; Table 2). The West Domain is still structurally complex with a symmetrical graben controlled by both N- and S-dipping faults (Fig. 6a; Table 2). Possible links between West Domain structure and pre-existing basement structure and composition are discussed below.

Timescales of growth and linkage of the rift border fault system

Border fault systems are common in most rift systems [e.g. *Ebinger*, 1989; *Schlische*, 1993], however, the timescales of their development are not well understood. In the Corinth Rift, we can now constrain these timescales. The southern margin of the modern Corinth Rift is characterized by numerous right stepping en echelon N-dipping faults that make up the border fault system (Fig. 5). Small and partially-linked depocentres form in the hanging wall of many of these faults by ca. 340 ka (Figs. 8 and 9). Over time these depocentres show diachronous growth in size and thickness (Fig. 9b) eventually merging to form a single large depocentre (Fig. 9c). Similar syn-rift sediment distributions have been seen in a number of rift basins recording the growth and linkage of rift fault systems [e.g. *Schlische*, 1993; *Gupta et al.*, 1998; *Morley,* 1999; *Contreras et al.*, 2000; *Wilson et al.*, 2009], but at lower resolutions and with less precise chronostratigraphic frameworks than presented here.

The profiles of maximum sediment accumulation rate (Figs. 10c and d) reflect hanging wall subsidence patterns of the major N-dipping faults along the southern rift margin. Initial along-strike variations in subsidence evolve to a centred but flattened bell-curve distribution (Fig. 10d), consistent with accumulation of displacement on coalescing fault segments that form a kinematically coherent fault system seen in other extensional systems [Fig. 12b and c; e.g. *Peacock and Sanderson*, 1991; *Dawers and Anders*, 1995; *Gupta and Scholz*, 2000; *Walsh et al.*, 2003a; *Taylor et al.*, 2004]. Hence, the individual en echelon N-dipping faults are likely to be linked at depth along the entire Gulf of Corinth (but disconnected from the Alkonides Gulf). The growth and linkage of discrete depocentres, increasing in length by ~40 m/kyr, suggests individual faults initially grew by rapid tip propagation before breaching of relay zones during segment linkage (Fig. 12b and c). These observations are consistent with observations by *Hemelsdaël and Ford* [2014] who show evidence for fault propagation and linkage of the East Eliki and Derveni Faults at the Akrata relay zone ca. 700-200 ka. This model of fault growth by propagation and segment linkage is at variance with instantaneous fault growth models where faults maintain a constant length and do not propagate as displacement builds [e.g. *Childs et al.,* 1995; *Walsh et al.*, 2002; *Paton et al.,* 2006].

Although the fault and depocentre linkage is a progressive process, it occurred rapidly and synchronously along-strike over a relatively short 300-500 kyr time interval (Fig. 12). Similar time scales of segment linkage are seen on the Rangitaiki Fault in the Whakatane Graben, which has evolved from isolated fault segments to a single coherent fault system over a period of ca. 400 kyr [*Taylor et al.*, 2004; *Bull et al.*, 2006; *Nixon et al.*, 2014]. The rapid linkage and establishment of a coherent border fault system is attributed to localization of deformation, a common observation of other rift fault systems [e.g. *Morley,* 1999; *Gawthorpe et al.*, 2003; *Walsh et al.*, 2003b; *Cowie et al.*, 2005; *Soliva and Schultz*, 2008] but rarely quantified.

Controls on migration, localization and along-strike variations in rift development

Rift migration, localization of deformation and evolution towards a simpler rift structure are significant processes in establishing the Corinth Rift structure. The following sequential evolutionary stages are identified (see Fig. 11):

1. Major northward migration of the rift (Fig. 11a to b).
2. Minor northward migration of the rift and a major change in rift symmetry towards asymmetry and development of the border fault system (Fig. 11b to c).
3. Rapid linkage and establishment of a coherent border fault system and associated depocentres, and localization of strain onto the border fault system (Fig. 11c to d).

The northward migration of the rift is sustained by sequential fault activity on both margins. *Ford et al*. [2013] illustrated this for the southern margin of the western Corinth Rift with migration between N-dipping faults (i.e. Kalavryta Fault to the Eliki Fault; Fig 11a-11c). Similar observations are seen at a number of margins including Iberia and Namibia [*Ranero and Pérez-Gussinyé,* 2010; *Mohammed et al.,* 2016]. For example, at the Iberian margin brittle deformation is accommodated by sequentially active faults that young and dip oceanward [e.g. *Wilson et al.*, 2001; *Ranero and Pérez-Gussinyé*, 2010]. Manatschal and Bernoulli [1999] propose that margin migration is driven by lithospheric cooling and strengthening during rifting. More recent thermo-mechanical models suggest that rift migration is controlled by lower crustal flow and that the extent of migration is a function of crustal rheology, strain softening and initial thermal structure [*Brune et al.*, 2014]. In Corinth, this early migration process may also be linked to the dynamics of the underlying subducting plate [e.g. *Tiberi et al.*, 2000; *Le Pourhiet et al.*, 2003; *Leeder et al.*, 2003], however these other margin examples demonstrate the process of migration can be part of the intrinsic rifting process.

Localization of deformation is consistent with both modelling results [e.g. *Behn et al*., 2002; *Huismans and Beaumont*, 2007] and other rift examples, including the Gulf of Suez and northern North Sea [e.g. *Gawthorpe et al*., 2003; *Cowie et al*., 2005]. However, these studies tend to observe migration of fault activity and localization towards the rift axis resulting in significant rift narrowing. In Corinth, a narrowing of the rift is not observed through time as indicated by the well constrained distribution of syn-rift sediments [illustrated in Fig. 11; *Ford et al.,* 2013]. Instead fault activity (although relatively minor) is maintained away from the zone of localization (the southern margin border fault system) as both southern and northern margins migrate northwards. Lithospheric-scale numerical models suggest that rift narrowing is caused by increasing geothermal gradients associated with lithosphere thinning [*Behn et al*., 2002], and/or frictional-plastic strain softening localizing on inherited weaknesses [*Huismans and Beaumont*, 2007]. The absence of rift narrowing suggests that these processes are not (yet?) dominant in the Corinth Rift, which maintains a narrow rift zone (20-40 km wide) throughout its history indicative of relatively low temperatures and a consequently strong lithosphere rheology [e.g. *Buck*, 1991; *Brun*, 1999].

Despite spatial and temporal variations in rift geometry and position over the last ca. 2 Ma, the Corinth Rift has clearly evolved towards a uniform asymmetric rift with deformation localized onto a few major N-dipping faults. The West Domain is the exception with strain still distributed across numerous N- and S-dipping faults and a contrasting evolution of strain rate relative to the rest of the rift with present-day extensional strain high in the west but relatively low in the past [e.g., *Bell et al*. 2011]. Variations in rift development can be caused by differences in underlying basement structure and composition through both reactivation of pre-existing structures [e.g. *Paton et al.*, 2006], or pervasive strength anisotropy deflecting the local stress field and affecting fault geometry [e.g. *Morley*, 2010; *Corti et al.*, 2013]. In Corinth, crustal thickness and basement composition/structure vary from east to west across the Hellenide fold-thrust belt that trends NNW-SSE across the Corinth Rift [e.g. *Skourtsos and Kranis*, 2009]. In the Central-East and East Domains (Fig. 5), an ESE structural fabric exists within the Parnassos nappe potentially pre-conditioning the basement for the localization and development of large E-W trending normal faults [*Taylor et al*., 2011]. However, in the Central-West and West Domains (Fig. 5), the Pindos nappe exhibits a strong NNW structural fabric that is highly oblique to the normal fault trends, hence, potentially inhibiting fault growth and favouring segmentation. This could contribute to the structural complexity and apparently immature rift development in the West Domain of the Gulf of Corinth.

In general, rift models fail to show many of the processes we have observed in the Corinth Rift, particularly the switch in fault polarity. This could be a result of the temporal resolution of numerical models which are typically on Myr timescales [e.g. *Huismans and Beaumont*, 2007; Brune et al., 2014].

Furthermore, some of these processes could be reflecting driving mechanisms associated with the Corinth Rift, such as the influences of the subducting slab or nearby major lithospheric boundaries (e.g. the North Anatolian Fault) that would change strain boundary conditions. Such influences on rifting are common and yet are typically not incorporated into numerical models, which use simple extensional boundary conditions, and thus should be considered for future modelling scenarios.

9. Conclusions

Using the largest seismic reflection dataset available, we have generated a unified stratigraphic and structural framework for the entire offshore Corinth Rift. We document variations in rift depocentre development and fault activity at unprecedented 100 kyr time scales, producing a high precision history of rift evolution over the past ca. 2 Myr.

The most significant structural change is the rapid transition from a structurally complex rift to a predominantly asymmetric rift over a 300 kyr period, starting at ca. 620 ka. Since ca. 620 ka, two phases of offshore rift development have dominated: 1) a change in rift symmetry; and then 2) progressive localization of deformation. The change in rift symmetry involved rapid (~200-300 kyr period) yet progressive transfer of deformation from S-dipping to N-dipping faults causing depocentre migration and the generation of a basin-wide syn-rift unconformity. Depocentres developing in the hanging walls of the N-dipping faults grew laterally at rates of ~40 m/kyr as the uniform asymmetric rift became established at ca. 340 ka. Growth and linkage of individual N-dipping faults controlled depocentre development, and a coherent, linked border-fault system was established rapidly (over a 300-500 kyr period) resulting in a single depocentre by ca. 130 ka with maximum sediment accumulation now in the centre of the rift.

This study illustrates that shifts in strain distribution within rifts can occur rapidly, on 100 kyr timescales. Strain localization can be synchronous throughout a rift once a uniform asymmetry has been established, allowing rapid growth and linkage of faults to form the rift border fault system. This process is progressive and can occur very early in a rift's history, in this case <4-5 Myr into rift history. We show that the rate of fault and depocentre linkage can be measured at very high temporal (ca. 100 kyr) and spatial (ca. 1 km) resolutions, where sediment supply is sufficient. Rift migration, an evolution towards asymmetry rather than symmetry and a rapid change in dominant fault polarity within a rift are not typically generated in simple rift models, yet may be a significant part of the rift evolution process.

10. Acknowledgments

We acknowledge funding from NERC (grants NE/J006564/1, NER/B/S/2001/00269), and the Royal Society. We thank the positive and constructive reviews of Douglas Paton, Chris Morley and an anonymous reviewer. The authors are grateful to Cindy Ebinger and Patience Cowie for their helpful comments and encouragement. We also thank HCMR and all the participants of an ECORD funded Corinth workshop whose fruitful discussions helped focus key ideas. All data used are documented in listed references, tables and supplements.

11. References

Ackermann, R. V., R. W. Schlische, and M. O. Withjack (2001), The geometric and statistical evolution of normal fault systems: an experimental study of the effects of mechanical layer thickness on scaling laws, *J. Struct. Geol.*, *23*(11), 1803–1819, doi:10.1016/S0191-8141(01)00028-1.

Aragón-Arreola, M., M. Morandi, A. Martín-Barajas, L. Delgado-Argote, and A. González-Fernández (2005), Structure of the rift basins in the central Gulf of California: Kinematic implications for oblique rifting, *Tectonophysics*, *409*(1-4), 19–38, doi:10.1016/j.tecto.2005.08.002.

Armijo, R., B. Meyer, G. C. P. King, A. Rigo, and D. Papanastassiou (1996), Quaternary evolution of the Corinth Rift and its implications for the Late Cenozoic evolution of the Aegean, *Geophys. J. Int.*, *126*(1), 11–53, doi:10.1111/j.1365-246X.1996.tb05264.x.

Armijo, R., B. Meyer, A. Hubert, and A. Barka (1999), Westward propagation of the North Anatolian fault into the northern Aegean: Timing and kinematics, *Geology*, *27*(3), 267–270, doi:10.1130/0091-7613(1999)027.

Avallone, A., P. Briole, A. M. Agatza-Balodimou, H. Billiris, O. Charade, C. Mitsakaki, A. Nercessian, K. Papazissi, D. Paradissis, and G. Veis (2004), Analysis of eleven years of deformation measured by GPS in the Corinth Rift Laboratory area, *Comptes Rendus Geosci.*, *336*(4-5), 301–311, doi:10.1016/j.crte.2003.12.007.

Backert, N., M. Ford, and F. Malartre (2010), Architecture and sedimentology of the Kerinitis Gilbert-type fan delta, Corinth Rift, Greece, *Sedimentology*, *57*(2), 543–586, doi:10.1111/j.1365-3091.2009.01105.x.

Beckers, A., A. Hubert-Ferrari, C. Beck, S. Bodeux, E. Tripsanas, D. Sakellariou, and M. De Batist (2015), Active faulting at the western tip of the Gulf of Corinth, Greece, from high-resolution seismic data, *Mar. Geol.*, *360*, 55–69, doi:10.1016/j.margeo.2014.12.003.

Behn, M. D., J. Lin, and M. T. Zuber (2002), A continuum mechanics model for normal faulting using a strain-rate softening rheology: implications for thermal and rheological controls on continental and oceanic rifting, *Earth Planet. Sci. Lett.*, *202*(3-4), 725–740, doi:10.1016/S0012-821X(02)00792-6.

Bell, R. E., L. C. McNeill, J. M. Bull, and T. J. Henstock (2008), Evolution of the offshore western Gulf of Corinth, *Geol. Soc. Am. Bull.*, *120*(1-2), 156–178, doi:10.1130/B26212.1.

Bell, R. E., L. C. McNeill, J. M. Bull, T. J. Henstock, R. E. L. Collier, and M. R. Leeder (2009), Fault architecture, basin structure and evolution of the Gulf of Corinth Rift, central Greece, *Basin Res.*, *21*(6), 824–855, doi:10.1111/j.1365-2117.2009.00401.x.

Bell, R. E., L. C. McNeill, T. J. Henstock, and J. M. Bull (2011), Comparing extension on multiple time and depth scales in the Corinth Rift, Central Greece, *Geophys. J. Int.*, *186*(2), 463–470, doi:10.1111/j.1365-246X.2011.05077.x.

Bell, R. E., C. A.-L. Jackson, P. S. Whipp, and B. Clements (2014), Strain migration during multiphase extension: Observations from the northern North Sea, *Tectonics*, *33*(10), 1936–1963, doi:10.1002/2014TC003551.

Bernard, P. et al. (2006), Seismicity, deformation and seismic hazard in the western rift of Corinth: New insights from the Corinth Rift Laboratory (CRL), *Tectonophysics*, *426*(1-2), 7–30, doi:10.1016/j.tecto.2006.02.012.

Bosworth, W., P. Huchon, and K. McClay (2005), The Red Sea and Gulf of Aden Basins, *J. African Earth Sci.*, *43*(1-3), 334–378, doi:10.1016/j.jafrearsci.2005.07.020.

Briole, P., A. Rigo, H. Lyon-Caen, J. C. Ruegg, K. Papazissi, C. Mitsakaki, A. Balodimou, G. Veis, D. Hatzfeld, and A. Deschamps (2000), Active deformation of the Corinth rift, Greece: Results from repeated Global Positioning System surveys between 1990 and 1995, *J. Geophys. Res.*, *105*(B11), 25605, doi:10.1029/2000JB900148.

Brun, J. (1999), Narrow rifts versus wide rifts: inferences for the mechanics of rifting from laboratory experiments, *Philos. Trans. R. Soc. A Math. Phys. Eng. Sci.*, *357*(1753), 695–712, doi:10.1098/rsta.1999.0349.

Brune, S., C. Heine, M. Pérez-Gussinyé, and S. V Sobolev (2014), Rift migration explains continental margin asymmetry and crustal hyper-extension., *Nat. Commun.*, *5*, 4014, doi:10.1038/ncomms5014.

Buck, W. R. (1991), Models of Continental Lithosphere Extension, *J. Geophys. Res.*, *96*(B12), 161–178.

Bull, J. M., P. M. Barnes, G. Lamarche, D. J. Sanderson, P. a. Cowie, S. K. Taylor, and J. K. Dix (2006), High-resolution record of displacement accumulation on an active normal fault: implications for models of slip accumulation during repeated earthquakes, *J. Struct. Geol.*, *28*(7), 1146–1166, doi:10.1016/j.jsg.2006.03.006.

Clement, C., 2000. Imagerie sismique crustale de la subduction Hellenique et du Golfe de Corinth, *PhD thesis*, University Paris VII, Paris.

Charalampakis, M., V. Lykousis, D. Sakellariou, G. Papatheodorou, and G. Ferentinos (2014), The tectono-sedimentary evolution of the Lechaion Gulf, the south eastern branch of the Corinth graben, Greece, *Mar. Geol.*, *351*, 58–75, doi:10.1016/j.margeo.2014.03.014.

Clarke, P. J. et al. (1998), Crustal strain in Greece from repeated GPS measurements in the interval 1989-1997, *Geophys. J. Int.*, *135*(1), 195–214, doi:10.1046/j.1365-246X.1998.00633.x.

Collier, R., and G. Jones (2003), Rift sequences of the Southern Margin of the Gulf of Corinth (Greece) as exploration/production analogues, *AAPG Int. Conf.*

Collier, R. E. L. (1990), Eustatic and tectonic controls upon Quaternary coastal sedimentation in the Corinth Basin, Greece, *J. Geol. Soc. London.*, *147*(2), 301–314, doi:10.1144/gsjgs.147.2.0301.

Collier, R. E. L., and C. J. Dart (1991), Neogene to Quaternary rifting, sedimentation and uplift in the Corinth Basin,Greece, *J. Geol. Soc. London.*, *148*(6), 1049–1065, doi:10.1144/gsjgs.148.6.1049.

Collier, R. E. L., M. R. Leeder, M. Trout, G. Ferentinos, E. Lyberis, and G. Papatheodorou (2000), High sediment yields and cool, wet winters: Test of last glacial paleoclimates in the northern Mediterranean, *Geology*, *28*(11), 999–1002, doi:10.1130/0091-7613(2000)28<999:HSYACW>2.0.CO;2.

Contreras, J., M. H. Anders, and C. H. Scholz (2000), Growth of a normal fault system: observations from the Lake Malawi basin of the east African rift, *J. Struct. Geol.*, *22*(2), 159–168, doi:10.1016/S0191-8141(99)00157-1.

Corti, G., M. Philippon, F. Sani, D. Keir, and T. Kidane (2013), Re-orientation of the extension direction and pure extensional faulting at oblique rift margins: Comparison between the Main Ethiopian Rift and laboratory experiments, *Terra Nov.*, *25*(5), 396–404, doi:10.1111/ter.12049.

Cowie, P. A., S. Gupta, and N. H. Dawers (2000), Implications of fault array evolution for synrift depocentre development: insights from a numerical fault growth model, *Basin Res.*, *12*(3-4), 241–261.

Cowie, P. A., J. Underhill, M. Behn, J. Lin, and C. Gill (2005), Spatio-temporal evolution of strain accumulation derived from multi-scale observations of Late Jurassic rifting in the northern North Sea: A critical test of models for lithospheric extension, *Earth Planet. Sci. Lett.*, *234*(3-4), 401–419, doi:10.1016/j.epsl.2005.01.039.

Cowie, P. A., G. P. Roberts, and E. Mortimer (2007), Strain localization within fault arrays over timescales of 100–107 years, in *Tectonic faults: agents of change on a dynamic Earth*, pp. 47–78.

Davies, R., P. England, B. Parsons, H. Billiris, D. Paradissis, and G. Veis (1997), Geodetic strain of Greece in the interval 1892–1992, *J. Geophys. Res.*, *102*(B11), 24571, doi:10.1029/97JB01644.

Dawers, N. H., and M. H. Anders (1995), Displacement – length scaling and fault linkage, *J. Struct. Geol.*, *17*, 607–614.

Doutsos, T., N. Kontopoulos, and G. Poulimenos (1988), The Corinth-Patras rift as the initial stage of continental fragmentation behind an active island arc (Greece), *Basin Res.*, *1*(3), 177–190.

Ebinger, C., and C. Scholz (2012), Continental rift basins: the East African perspective, *Tectonics Sediment. Basins Recent Adv.*, 185–208.

Ebinger, C. J. (1989), Geometric and kinematic development of border faults and accommodation zones, Kivu-Rusizi rift, Africa, *Tectonics*, *8*(1), 117–133.

Ford, M., C. Le Carlier de Veslud, and O. Bourgeois (2007), Kinematic and geometric analysis of fault-related folds in a rift setting: The Dannemarie basin, Upper Rhine Graben, France, *J. Struct. Geol.*, *29*(11), 1811–1830, doi:10.1016/j.jsg.2007.08.001.

Ford, M., S. Rohais, E. A. Williams, S. Bourlange, D. Jousselin, N. Backert, and F. Malartre (2013), Tectono-sedimentary evolution of the western Corinth rift (Central Greece), *Basin Res.*, *25*(1), 3–25, doi:10.1111/j.1365-2117.2012.00550.x.

Fossen, H., and J. Hesthammer (1998), Structural geology of the Gullfaks Field, northern North Sea, *Geol. Soc. London, Spec. Publ.*, *127*(1), 231–261, doi:10.1144/GSL.SP.1998.127.01.16.

Gawthorpe, R. L., and M. R. Leeder (2000), Tectono-sedimentary evolution of active extensional basins, *Basin Res.*, *12*(3-4), 195–218.

Gawthorpe, R. L., A. J. Fraser, and R. E. L. Collier (1994), Sequence stratigraphy in active extensional basins: implications for the interpretation of ancient basin-fills, *Mar. Pet. Geol.*, *11*(6), 642–658, doi:10.1016/0264-8172(94)90021-3.

Gawthorpe, R. L., C. A. L. Jackson, M. J. Young, I. R. Sharp, A. R. Moustafa, and C. W. Leppard (2003), Normal fault growth, displacement localisation and the evolution of normal fault populations: The Hammam Faraun fault block, Suez rift, Egypt, *J. Struct. Geol.*, *25*(6), 883–895, doi:10.1016/S0191-8141(02)00088-3.

Goldhammer, R.K., (1997), Compaction and decompaction algorithms for sedimentary carbonates. *J. Sedimentary Research,* 67 (1), 26-35.

Gupta, A., and C. H. Scholz (2000), A model of normal fault interaction based on observations and theory, *J. Struct. Geol.*, *22*(7), 865–879, doi:10.1016/S0191-8141(00)00011-0.

Gupta, S., P. A. Cowie, N. H. Dawers, and J. R. A. Underhill (1998), Mechanism to explain rift basin subsidence and stratigraphic patterns through fault array evolution, *Geology*, *26*, 595–598.

Hayward, N. J., and C. J. Ebinger (1996), Variations in the along-axis segmentation of the Afar Rift system, *Tectonics*, *15*(2), 244, doi:10.1029/95TC02292.

Hemelsdaël, R., and M. Ford (2014), Relay zone evolution: a history of repeated fault propagation and linkage, central Corinth rift, Greece, *Basin Res.*, 1–23, doi:10.1111/bre.12101.

Huismans, R. S., and C. Beaumont (2007), Roles of lithospheric strain softening and heterogeneity in determining the geometry of rifts and continental margins, *Geol. Soc. London, Spec. Publ.*, *282*(1), 111–138, doi:10.1144/SP282.6.

Jolivet, L., J. M. Daniel, C. Truffert, and B. Goffé (1994), Exhumation of deep crustal metamorphic rocks and crustal extension in arc and back-arc regions, *Lithos*, *33*(1-3), 3–30, doi:10.1016/0024-4937(94)90051-5.

Leeder, M. R., and G. H. Mack (2009), Basin-Fill Incision, Rio Grande and Gulf of Corinth Rifts: Convergent Response to Climatic and Tectonic Drivers, in *Sedimentary Processes, Environments and Basins*, pp. 9–27.

Leeder, M. R., R. E. L. Collier, L. H. Abdul Aziz, M. Trout, G. Ferentinos, G. Papatheodorou, and E. Lyberis (2002), Tectono-sedimentary processes along an active marine/lacustrine half-graben margin: Alkyonides Gulf, E. Gulf of Corinth, Greece, *Basin Res.*, *14*(1), 25–41, doi:10.1046/j.1365-2117.2002.00164.x.

Leeder, M. R., L. C. McNeill, R. E. L. Collier, C. Portman, P. J. Rowe, J. E. Andrews, and R. L. Gawthorpe (2003), Corinth Rift margin uplift: new evidence from Late Quaternary marine shorelines, *Geophys. Res. Lett.*, *30*(12), 1611, doi:10.1029/2003GL017382.

Leeder, M. R., C. Portman, J. E. Andrews, R. E. L. Collier, E. Finch, R. L. Gawthorpe, L. C. McNeill, M. Perez-Arlucea, and P. Rowe (2005), Normal faulting and crustal deformation, Alkyonides Gulf and Perachora peninsula, eastern Gulf of Corinth rift, Greece, *J. Geol. Soc. London.*, *162*(3), 549–561, doi:10.1144/0016-764904-075.

Leeder, M. R., G. H. Mack, A. T. Brasier, R. R. Parrish, W. C. McIntosh, J. E. Andrews, and C. E. Duermeijer (2008), Late-Pliocene timing of Corinth (Greece) rift-margin fault migration, *Earth Planet. Sci. Lett.*, *274*(1-2), 132–141, doi:10.1016/j.epsl.2008.07.006.

Leeder, M. R., D. F. Mark, R. L. Gawthorpe, H. Kranis, S. Loveless, N. Pedentchouk, E. Skourtsos, J. Turner, J. E. Andrews, and M. Stamatakis (2012), A “Great Deepening”: Chronology of rift climax, Corinth rift, Greece, *Geology*, *40*(11), 999–1002, doi:10.1130/G33360.1.

Lykousis, V., D. Sakellariou, I. Moretti, and H. Kaberi (2007), Late Quaternary basin evolution of the Gulf of Corinth: Sequence stratigraphy, sedimentation, fault–slip and subsidence rates, *Tectonophysics*, *440*(1-4), 29–51, doi:10.1016/j.tecto.2006.11.007.

Kornsawan, A. and C. K. Morley (2002), The origin and evolution of complex transfer zones (graben shifts) in conjugate fault systems around the Funan Field, Pattani basin, Gulf of Thailand. *J. Struct. Geol.*, 24, 435-449.

Manatschal, G., and D. Bernoulli (1999), Architecture and tectonic evolution of nonvolcanic margins: Present-day Galicia and ancient Adria, *Tectonics*, *18*(6), 1099–1119, doi:10.1029/1999TC900041.

Mansfield, C., and J. Cartwright (2001), Fault growth by linkage: observations and implications from analogue models, *J. Struct. Geol.*, *23*, 745–763.

McClay, K., T. Dooley, P. Whitehouse, and M. Mills (2002), 4-D evolution of rift systems: Insights from scaled physical models, *Am. Assoc. Pet. Geol. Bull.*, *86*(6), 935–959.

McKenzie, D. (1972), Active Tectonics of the Mediterranean Region, *Geophys. J. Int.*, *30*(2), 109–185, doi:10.1111/j.1365-246X.1972.tb02351.x.

McKenzie, D. (1978), Active tectonics of the Alpine--Himalayan belt: the Aegean Sea and surrounding regions, *Geophys. J. Int.*, *55*(1), 217–254, doi:10.1111/j.1365-246X.1978.tb04759.x.

McNeill, L., D. Sakellariou, and C. Nixon (2014), Drilling to Resolve the Evolution of the Corinth Rift, *Eos, Trans. Am. Geophys. Union*, *95*(20), 170–170, doi:10.1002/2014EO200009.

McNeill, L. C., and R. E. L. Collier (2004), Uplift and slip rates of the eastern Eliki fault segment, Gulf of Corinth, Greece, inferred from Holocene and Pleistocene terraces, *J. Geol. Soc. London.*, *161*(1), 81–92, doi:10.1144/0016-764903-029.

McNeill, L. C., C. J. Cotterill, T. J. Henstock, J. M. Bull, A. Stefatos, R. E. L. Collier, G. Papatheoderou, G. Ferentinos, and S. E. Hicks (2005), Active faulting within the offshore western Gulf of Corinth, Greece: Implications for models of continental rift deformation, *Geology*, *33*(4), 241–244, doi:10.1130/G21127.1.

Mohammed, M., D. Paton, R. E. L. Collier, N. Hodgson, and M. Negonga (2016), Interaciton of crustal heterogeneity and lithospheric processes in determining passive margin architecture on the southern Namibian margin, *Geol. Soc. London, Spec. Publ.*, 438, doi:10.1144/SP438.9.

Moretti, I., V. Lykousis, D. Sakellariou, J. Y. Reynaud, B. Benziane, and A. Prinzhoffer (2004), Sedimentation and subsidence rate in the Gulf of Corinth: what we learn from the Marion Dufresne’s long-piston coring, *Comptes Rendus - Geosci.*, *336*(4-5), 291–299, doi:10.1016/j.crte.2003.11.011.

Morley, C.K. (1999), Patterns of displacement along large normal faults: Implicaitons for basin evolution and fault propagation, based on examples from East Africa. *AAPG Bulletin,* 83, p. 613-634.

Morley, C. K. (2010), Stress re-orientation along zones of weak fabrics in rifts: An explanation for pure extension in “oblique” rift segments?, *Earth Planet. Sci. Lett.*, *297*(3-4), 667–673, doi:10.1016/j.epsl.2010.07.022.

Morley, C.K., P. Vanhauwaert, and M. De Batist (2000), Evidence for high frequency cyclic fault activity from high resolution seismic reflection survey, Rukwa Rift, Tanzania. *J. Geol. Soc. London.,* 157, 983-984.

Nelson, R. A., T. L. Patton and C. K. Morley (1992), Rift-segement interaction and its relation to hydrocarbon exploration in continental rift systems. *AAPG Bulletin*, 76, 1153-1169.

Nixon, C. W., D. J. Sanderson, and J. M. Bull (2011), Deformation within a strike-slip fault network at Westward Ho!, Devon U.K.: Domino vs conjugate faulting, *J. Struct. Geol.*, *33*(5), 833–843, doi:10.1016/j.jsg.2011.03.009.

Nixon, C. W., J. M. Bull, and D. J. Sanderson (2014), Localized vs distributed deformation associated with the linkage history of an active normal fault, Whakatane Graben, New Zealand, *J. Struct. Geol.*, *69,* 266-280, doi:10.1016/j.jsg.2014.06.005.

Ori, G. G. (1989), Geologic history of the extensional basin of the Gulf of Corinth (?Miocene-Pleistocene), Greece, *Geology*, *17*(10), 918–921, doi:10.1130/0091-7613(1989)017<0918:GHOTEB>2.3.CO;2.

Paton, D.A. (2006), Influence of crustal heterogeneity on normal fault dimensions and evolution: southern South Africa extensional system, *J. Struct. Geol., 28(5),* 868-886.

Paton, D. A., D. I. M. Macdonald, and J. R. Underhill (2006), Applicability of thin or thick skinned structural models in a region of multiple inversion episodes; southern South Africa, *J. Struct. Geol.*, *28*(11), 1933–1947, doi:10.1016/j.jsg.2006.07.002.

Patton, T. L., A. R. Moustafa, R. A. Nelson, and S. A. Abdine (1994), Tectonic Evolution and Structural Setting of the Suez Rift: Chapter 1: Part I. Type Basin: Gulf of Suez, *Inter. Rift Basins*, *59*, 9–55.

Peacock, D. C. P., and D. J. Sanderson (1991), Displacements, segment linkage and relay ramps in normal fault zones, *J. Struct. Geol.*, *13*(6), 721–733, doi:10.1016/0191-8141(91)90033-F.

Le Pourhiet, L., E. Burov, and I. Moretti (2003), Initial crustal thickness geometry controls on the extension in a back arc domain: Case of the Gulf of Corinth, *Tectonics*, *22*(4), doi:10.1029/2002TC001433.

Ranero, C. R., and M. Pérez-Gussinyé (2010), Sequential faulting explains the asymmetry and extension discrepancy of conjugate margins., *Nature*, *468*(7321), 294–9, doi:10.1038/nature09520.

Roberts, G. P., S. L. Houghton, C. Underwood, I. Papanikolaou, P. A. Cowie, P. van Calsteren, T. Wigley, F. J. Cooper, and J. M. McArthur (2009), Localization of Quaternary slip rates in an active rift in 10 5 years: An example from central Greece constrained by 234 U- 230 Th coral dates from uplifted paleoshorelines, *J. Geophys. Res.*, *114*(B10), B10406, doi:10.1029/2008JB005818.

Roberts, S., and J. Jackson (1991), Active normal faulting in central Greece: an overview, *Geol. Soc. London, Spec. Publ.*, *56*(1), 125–142, doi:10.1144/GSL.SP.1991.056.01.09.

Rohais, S., R. Eschard, M. Ford, F. Guillocheau, and I. Moretti (2007), Stratigraphic architecture of the Plio-Pleistocene infill of the Corinth Rift: Implications for its structural evolution, *Tectonophysics*, *440*(1-4), 5–28, doi:10.1016/j.tecto.2006.11.006.

Rosendahl, B.R., (1987), Architecture of continental rifts with special reference to East Africa. *Ann. Rev. Earth Planet. Sci.,* 1987, 445-503

Sachpazi, M., C. Clément, M. Laigle, A. Hirn, and N. Roussos (2003), Rift structure, evolution, and earthquakes in the Gulf of Corinth, from reflection seismic images, *Earth Planet. Sci. Lett.*, *216*(3), 243–257, doi:10.1016/S0012-821X(03)00503-X.

Sakellariou, D., V. Lykousis, S. Alexandri, H. Kaberi, G. Rousakis, P. Nomikou, P. Georgiou, and D. Ballas (2007), Faulting, seismic-stratigraphic architecture and Late Quaternary evolution of the Gulf of Alkyonides Basin-East Gulf of Corinth, Central Greece, *Basin Res.*, *19*(2), 273–295, doi:10.1111/j.1365-2117.2007.00322.x.

Schlische, R. W. (1993), Anatomy and evolution of the Triassic-Jurassic Continental Rift System, eastern North America, *Tectonics*, *12*(4), 1026, doi:10.1029/93TC01062.

Schlische, R. W., and M. O. Withjack (2009), Origin of fault domains and fault-domain boundaries (transfer zones and accommodation zones) in extensional provinces: Result of random nucleation and self-organized fault growth, *J. Struct. Geol.*, *31*(9), 910–925, doi:10.1016/j.jsg.2008.09.005.

Skourlis, K., and T. Doutsos (2003), The Pindos Fold-and-thrust belt (Greece): inversion kinematics of a passive continental margin, *Int. J. Earth Sci.*, *92*(6), 891–903, doi:10.1007/s00531-003-0365-4.

Skourtsos, E., and H. Kranis (2009), Structure and evolution of the western Corinth Rift, through new field data from the Northern Peloponnesus, *Geol. Soc. London, Spec. Publ.*, *321*(1), 119–138, doi:10.1144/SP321.6.

Soliva, R., and R. A. Schultz (2008), Distributed and localized faulting in extensional settings: Insight from the North Ethiopian Rift–Afar transition area, *Tectonics*, *27*(2), TC2003, doi:10.1029/2007TC002148.

Stefatos, A., G. Papatheodorou, G. Ferentinos, M. Leeder, and R. Collier (2002), Seismic reflection imaging of active offshore faults in the Gulf of Corinth: their seismotectonic significance, *Basin Res.*, *14*(4), 487–502, doi:10.1046/j.1365-2117.2002.00176.x.

Taylor, B., J. R. Weiss, A. M. Goodliffe, M. Sachpazi, M. Laigle, and A. Hirn (2011), The structures, stratigraphy and evolution of the Gulf of Corinth rift, Greece, *Geophys. J. Int.*, *185*(3), 1189–1219, doi:10.1111/j.1365-246X.2011.05014.x.

Taylor, S. K., J. M. Bull, G. Lamarche, and P. M. Barnes (2004), Normal fault growth and linkage in the Whakatane Graben, New Zealand, during the last 1.3 Myr, *J. Geophys. Res.*, *109*(B2), B02408, doi:10.1029/2003JB002412.

Tiberi, C. et al. (2000), Crustal and upper mantle structure beneath the Corinth rift (Greece) from a teleseismic tomography study, *J. Geophys. Res.*, *105*(B12), 28159, doi:10.1029/2000JB900216.

Walsh, J. J. et al. (2001), Geometric controls on the evolution of normal fault systems, *Geol. Soc. London, Spec. Publ.*, *186*(1), 157–170, doi:10.1144/GSL.SP.2001.186.01.10.

Walsh, J. J., W. R. Bailey, C. Childs, a. Nicol, and C. G. Bonson (2003a), Formation of segmented normal faults: A 3-D perspective, *J. Struct. Geol.*, *25*(8), 1251–1262, doi:10.1016/S0191-8141(02)00161-X.

Walsh, J. J., C. Childs, J. Imber, T. Manzocchi, J. Watterson, and P. A. R. Nell (2003b), Strain localisation and population changes during fault system growth within the Inner Moray Firth, Northern North Sea, *J. Struct. Geol.*, *25*(2), 307–315, doi:10.1016/S0191-8141(02)00028-7.

Wilson, P., D. Hodgetts, F. Rarity, R. L. Gawthorpe, and I. R. Sharp (2009), Structural geology and 4D evolution of a half-graben: New digital outcrop modelling techniques applied to the Nukhul half-graben, Suez rift, Egypt, *J. Struct. Geol.*, *31*(3), 328–345, doi:10.1016/j.jsg.2008.11.013.

Wilson, R. C. L., G. Manatschal, and S. Wise (2001), Rifting along non-volcanic passive margins: stratigraphic and seismic evidence from the Mesozoic successions of the Alps and western Iberia, *Geol. Soc. London, Spec. Publ.*, *187*(1), 429–452, doi:10.1144/GSL.SP.2001.187.01.21.

Wood, A.M., D. A. Paton, and R. E. Ll. Collier (2015), Understanding regional scale structural uncertainty: The onshore Gulf of Corinth Rift as a hydrocarbon exploration analogue. *Interpretation.* 3 (4), SAC35-SAC53.

Zelt, B.C., B. Taylor, J. R. Weiss, A. M. Goodliffe, M. Sachpazi and A. Hirn (2004), Streamer topography velocity models for the Gulf of Corinth and Gulf of Itea, Greece. *Geophys. J. Int.,* 159, 333-346.

Figure Captions

Figure 1. Structural map of the Corinth Rift, illustrating the new and refined offshore fault network interpreted in this study. Inset is a location map of the Corinth Rift within the tectonic framework of the Aegean. All major active faults offset 100 kyr horizon (see Fig. 3). Onshore faults are after *Ford et al.* [2008] in the west, *Skoutsos and Kranis* [2009] for the central rift, *Collier and Dart* [1991] and *Freyberg* [1973] in the east. Offshore faults in the Trizonia Basin are after *Beckers et al*. [2015]. Bathymetry data courtesy of the Hellenic Centre for Marine Research collected for R/V AEGAEO cruises [*Sakellariou et al.*, 2007].

Figure 2. Map showing the locations of seismic reflection profiles and details of the seismic sources used to constrain the chronostratigraphy and fault geometry throughout the Corinth Rift. The locations of the interpreted seismic profiles in Figures 3 and 4 are also shown.

Figure 3. Corinth Rift chronostratigraphic framework, applicable to the entire rift, derived from analysis of data in Figure 2 which reconciles all previous interpretations. a) Representative multichannel seismic reflection profile from the central Gulf of Corinth (R/V Maurice Ewing, 2001) illustrating the seismic stratigraphy, and modelled ages of alternating high and low amplitude packages within the upper Seismic Unit 2 (SU2), and correlation with ca. 100 kyr glacio-eustatic cycles. Packages are correlated to the sea level curve of *Bintanja and van der Wal* [2008] for the past ca. 620 kyr. The current depth of the Rion Strait sill is indicated. Inset box indicates location of close-ups illustrated in b) and c). b) and c) illustrate horizons (H1 – H6, U) on a conventional seismic reflection profile, and on a profile with an amplitude volume attribute (RMS) applied to highlight the contrasting marine and lacustrine packages (high and low amplitude respectively). d) Proposed horizon age (<620 kyr) model for the Corinth Rift.

Figure 4. a) Chronostratigraphic framework used in this study applied to a high resolution seismic reflection profile from the Alkyonides Gulf. Note how the tops

of clinoforms [C1-5; interpreted by *Leeder et al*., 2005] correlate with the marine transgressive horizons (H1-H5) which represent the base of the high amplitude marine packages. H6 is the base of the deepest marine package above unconformity U. This interpretation is consistent with *Bell et al*. [2009]. b) West to East along-rift high resolution seismic reflection profile illustrating how the chronostratigraphic framework from this study agrees with the interpretation of *Bell et al*. [2008]. The positions of profiles a) and b) are shown in Figure 2. Solid horizons represent interpretation from this study, dashed horizons are from previous studies. Uninterpreted profiles can be viewed in the supplementary information.

Figure 5. Fault map illustrating major faults offsetting seismic basement (depth illustrated by coloured contours) with the width of the offshore fault polygons proportional to the heave on the faults. The down-throw direction of the faults is shown. The offshore Corinth Rift is divided into five domains from west to east to illustrate along-strike variation in rift architecture (see text for further description). The location of a representative seismic profile from each domain illustrated in Figure 6 is shown by the solid grey lines. Fault names: TRI=Trizonia Fault, NEF=North Eratini Fault, SEF=South Eratini Fault, WCF=West Channel Fault, ECF=East Channel Fault, AIG=Aigion, DIA=Diakopto, GAL=Galaxidi, PMF=Pyrgaki-Mamoussia Fault, EEF=East Eliki Fault, WEF=West Eliki Fault, AKR=Akrata, DER=Derveni, LYK=Lykoporia, EXF=East Xylokastro Fault, WXF=West Xylokastro Fault, NKF=North Kiato Fault, LEX= Lechaion, HER=Heraion, PER=Perachora, STR=Strava, WAF=West Alkyonides Fault, EAF=East Alkyonides Fault, LIV=Livadostras, EDF=East Domvrena Fault, WDF=West Domvrena Fault, VRA=Vroma, EAN=East Antikyra, WAN=West Antikyra.

Figure 6. Interpreted seismic reflection profiles illustrating temporal-spatial changes in rift geometry and fault polarity along the Corinth Rift. Profiles a) to e) represent the West, Central-West, Central-East, East and Alkyonides Domains shown in Figure 5, respectively. North and south-dipping faults are shown in blue and red respectively, see Figure 5 for fault nomenclature. Horizons H1-6, U are labelled together with three syn-rift packages (yellow:

seabed-H4; red: H4-U; blue: U-basement). See Table 2 for age correlation and summary of changes in fault polarity between rift domains. Uninterpreted profiles can be viewed in the supplementary information.

Figure 7. Isochore maps derived from the entire seismic reflection data set (Fig. 2) for a) Seismic Unit 1 (SU1; ca. 1.5-2 Ma to 620ka) and b) Seismic Unit 2 (SU2; ca. 620ka to present day) illustrating major sediment depocentres and active faults. The fault polygons for each time period represent the cumulative heave on the faults within each time period. Fault nomenclature is as Figure 5. Note the localized depocentres controlled by the Galaxidi Fault in the Central-West Domain and both north and south-dipping faults in the East Domain during before ca. 620 ka. After ca. 620 ka the major north-dipping faults along the south shore of the Corinth Rift control the development of a laterally continuous depocentre (~50 km in length).

Figure 8. Isochore maps illustrating depocentre development over three time periods from ca. 620-340 ka: a) ca. 620-530 ka; b) ca. 530-420 ka; c) ca. 420-340 ka isochores. The fault polygons for each time period represent the cumulative heave on the faults since ca. 620 ka. Initially (a) discrete depocentres are controlled by both north and south-dipping faults. This is followed by a gradual migration from north to south (b and c) until all discrete depocentres are controlled by the southern margin north-dipping faults (c).

Figure 9. Isochore maps illustrating depocentre development over three time periods from ca. 340 ka to the present day: a) ca. 340-240 ka; b) ca. 240-130 ka; c) ca. 130 ka - present isochores. The fault polygons for time periods ca. 340-130 ka and ca. 130 ka - present represent the cumulative heave on the faults since ca. 340 ka and ca. 130 ka, respectively. Initially (a), numerous small depocentres (~4-8 km in length) are controlled by discrete north-dipping faults, along the southern margin of the Corinth Rift. These depocentres grow in size and become more linked with time (b and c) eventually forming a large continuous depocentre ~40 km in length (c), illustrating linkage of and localization on major north-dipping faults.

Figure 10. Spatial and temporal changes in the loci of sediment deposition within the offshore Corinth Rift. a) Changes in the maximum decompacted sediment thickness for the major time periods. Note the change from two major depocentres before ca. 620 ka to a single broad depocentre after ca. 620 ka (blue and red respectively). The present shoreline locations of major rivers are shown and labelled. b) and c) show the change in maximum decompacted sedimentation rate along the rift for six ca. 100 kyr glacio-eustatic cycles. The along-rift sedimentation becomes more uniform with time. d) Schematic map showing positions of major controlling faults in the Gulf of Corinth and Alkyonides Gulf. North and South dipping faults are shown in black and grey respectively. e) Changes in the loci of sedimentation before and since ca. 620 ka (blue and red stripe areas offshore respectively). Positions of major faults are shown in bold as well as locus of onshore Plio-Quaternary sedimentation and outcrop of pre-rift basement.

Figure 11. Plan view maps indicating evolution of Corinth Rift from inception ca. 4 Ma to present day. Inferred fault activity based on new insights from this study, previous offshore studies [*McNeill et al*., 2005; *Bell et al*., 2008, 2009] and correlations with recent onshore studies [*Leeder et al*., 2008, 2012; *Ford et al*., 2013; *Charalampakis et al*., 2014]. The distribution of well constrained syn-rift sediments is shown for each time period indicating the region of focused extension. See text for discussion of rift evolution.

Figure 12. 3-D block diagrams illustrating the development of a rift border fault system and associated depocentres.

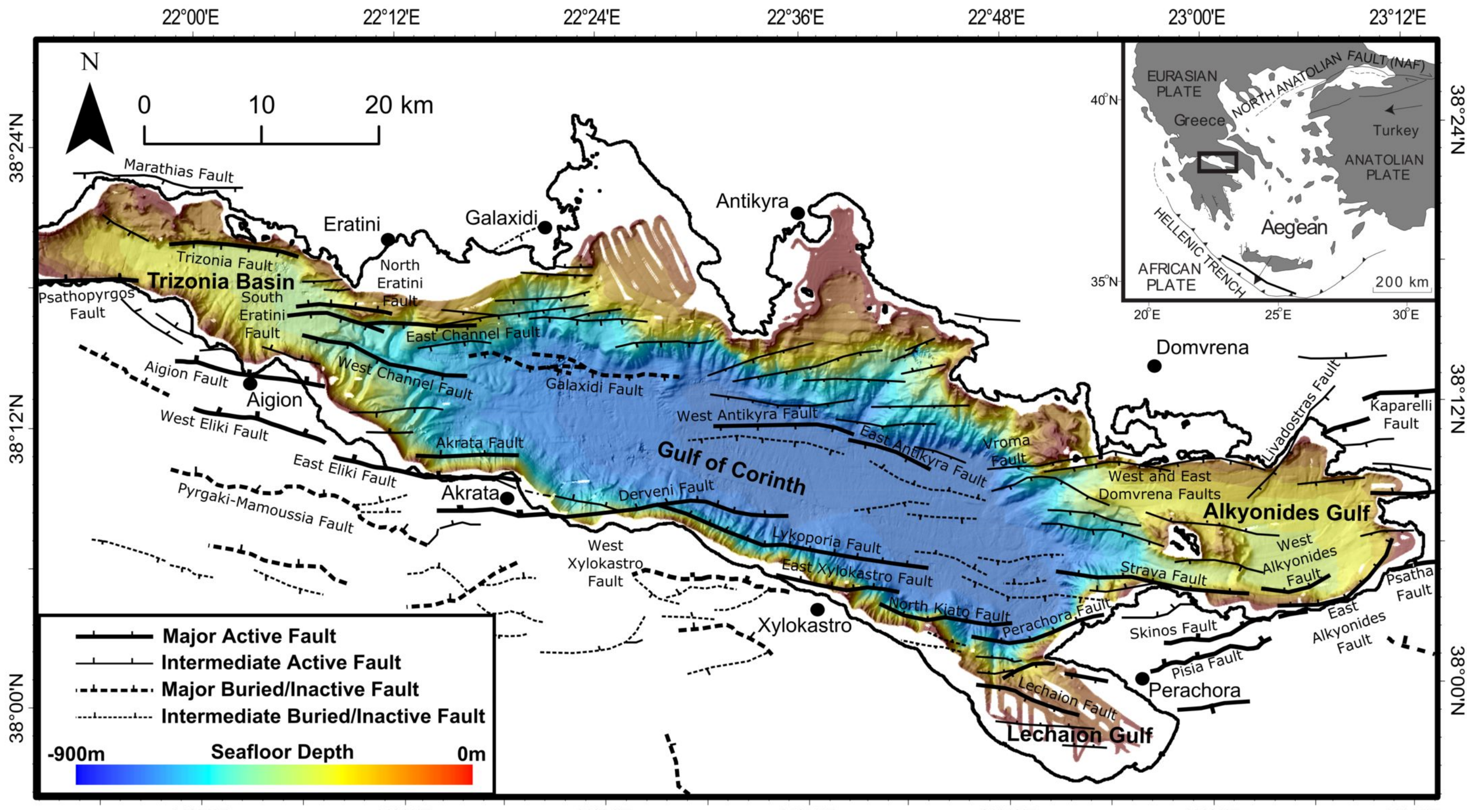

22°00'E
22°12'E
22°24'E
22°36'E
22°48'E
23°00'E
23°12'E
38°24'N
38°12'N
38°00'N
N
0
10
20 km
Marathias Fault
Trizonia Fault
Trizonia Basin
Psathopyrgos Fault
South Eratini Fault
North Eratini Fault
Eratini
Galaxidi
Antikyra
East Channel Fault
West Channel Fault
Galaxidi Fault
Aigion Fault
Aigion
West Eliki Fault
East Eliki Fault
Akrata Fault
Akrata
Pyrgaki-Mamoussia Fault
West Antikyra Fault
East Antikyra Fault
Gulf of Corinth
Derveni Fault
West Xylokastro Fault
Lykoporia Fault
East Xylokastro Fault
Xylokastro
North Kiato Fault
Perachora Fault
Vroma Fault
Domvrena
West and East Domvrena Faults
Livadostras Fault
Kaparelli Fault
Alkyonides Gulf
West Alkyonides Fault
Strava Fault
Skinos Fault
Pisia Fault
East Alkyonides Fault
Psatha Fault
Perachora
Lechaion Fault
Lechaion Gulf
EURASIAN PLATE
NORTH ANATOLIAN FAULT (NAF)
Greece
Turkey
ANATOLIAN PLATE
Aegean
HELLENIC TRENCH
AFRICAN PLATE
40°N
35°N
20°E
25°E
30°E
200 km
Major Active Fault
Intermediate Active Fault
Major Buried/Inactive Fault
Intermediate Buried/Inactive Fault
-900m
Seafloor Depth
0m

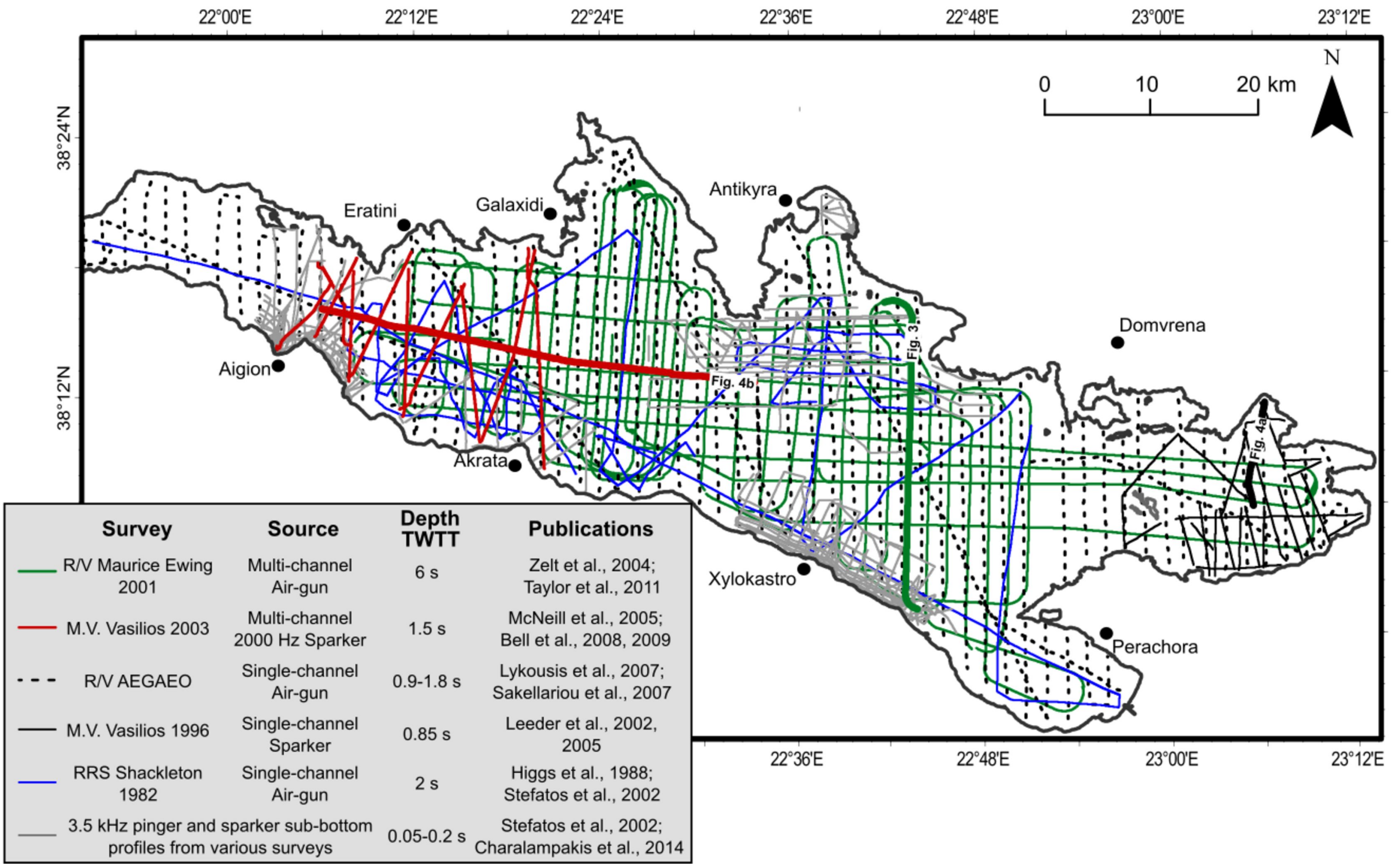

22°00'E
22°12'E
22°24'E
22°36'E
22°48'E
23°00'E
23°12'E
38°24'N
38°12'N
38°00'N
N
0
10
20 km
Eratini
Galaxidi
Antikyra
Domvrena
Aigion
Akrata
Xylokastro
Perachora
Fig. 4b
Fig. 3
Fig. 4a
Survey
Source
Depth TWTT
Publications
R/V Maurice Ewing 2001
Multi-channel Air-gun
6 s
Zelt et al., 2004; Taylor et al., 2011
M.V. Vasilios 2003
Multi-channel 2000 Hz Sparker
1.5 s
McNeill et al., 2005; Bell et al., 2008, 2009
R/V AEGAEO
Single-channel Air-gun
0.9-1.8 s
Lykousis et al., 2007; Sakellariou et al., 2007
M.V. Vasilios 1996
Single-channel Sparker
0.85 s
Leeder et al., 2002, 2005
RRS Shackleton 1982
Single-channel Air-gun
2 s
Higgs et al., 1988; Stefatos et al., 2002
3.5 kHz pinger and sparker sub-bottom profiles from various surveys
0.05-0.2 s
Stefatos et al., 2002; Charalampakis et al., 2014

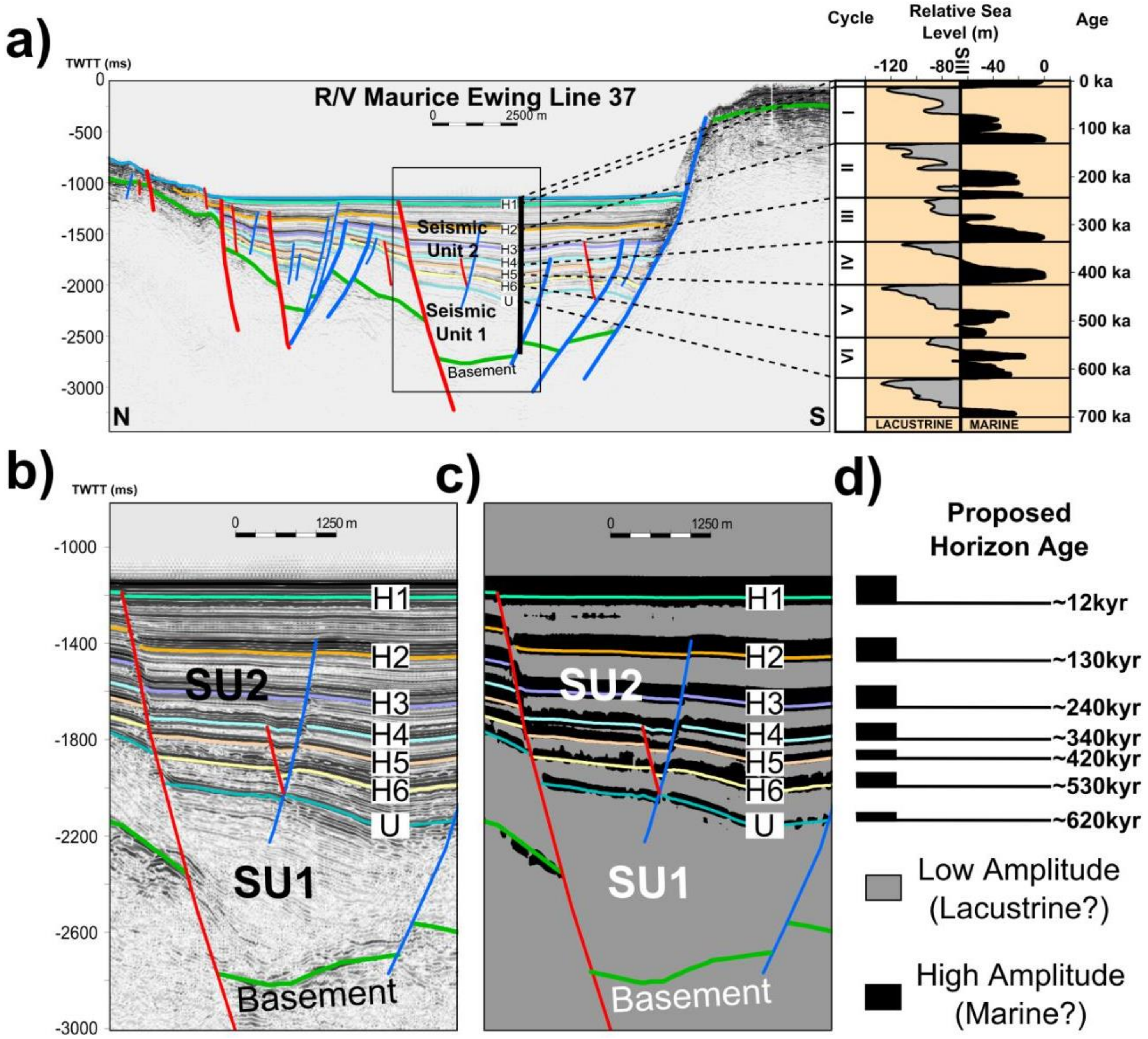

a)
TWTT (ms)
R/V Maurice Ewing Line 37
0 2500 m
Seismic Unit 2
Seismic Unit 1
Basement
H1
H2
H3
H4
H5
H6
U
N
S
Cycle
Relative Sea Level (m)
SILL
Age
-120 -80 -40 0
I
II
III
IV
V
VI
0 ka
100 ka
200 ka
300 ka
400 ka
500 ka
600 ka
700 ka
LACUSTRINE
MARINE
b)
TWTT (ms)
0 1250 m
SU2
SU1
Basement
c)
0 1250 m
SU2
SU1
Basement
d)
Proposed Horizon Age
~12kyr
~130kyr
~240kyr
~340kyr
~420kyr
~530kyr
~620kyr
Low Amplitude (Lacustrine?)
High Amplitude (Marine?)

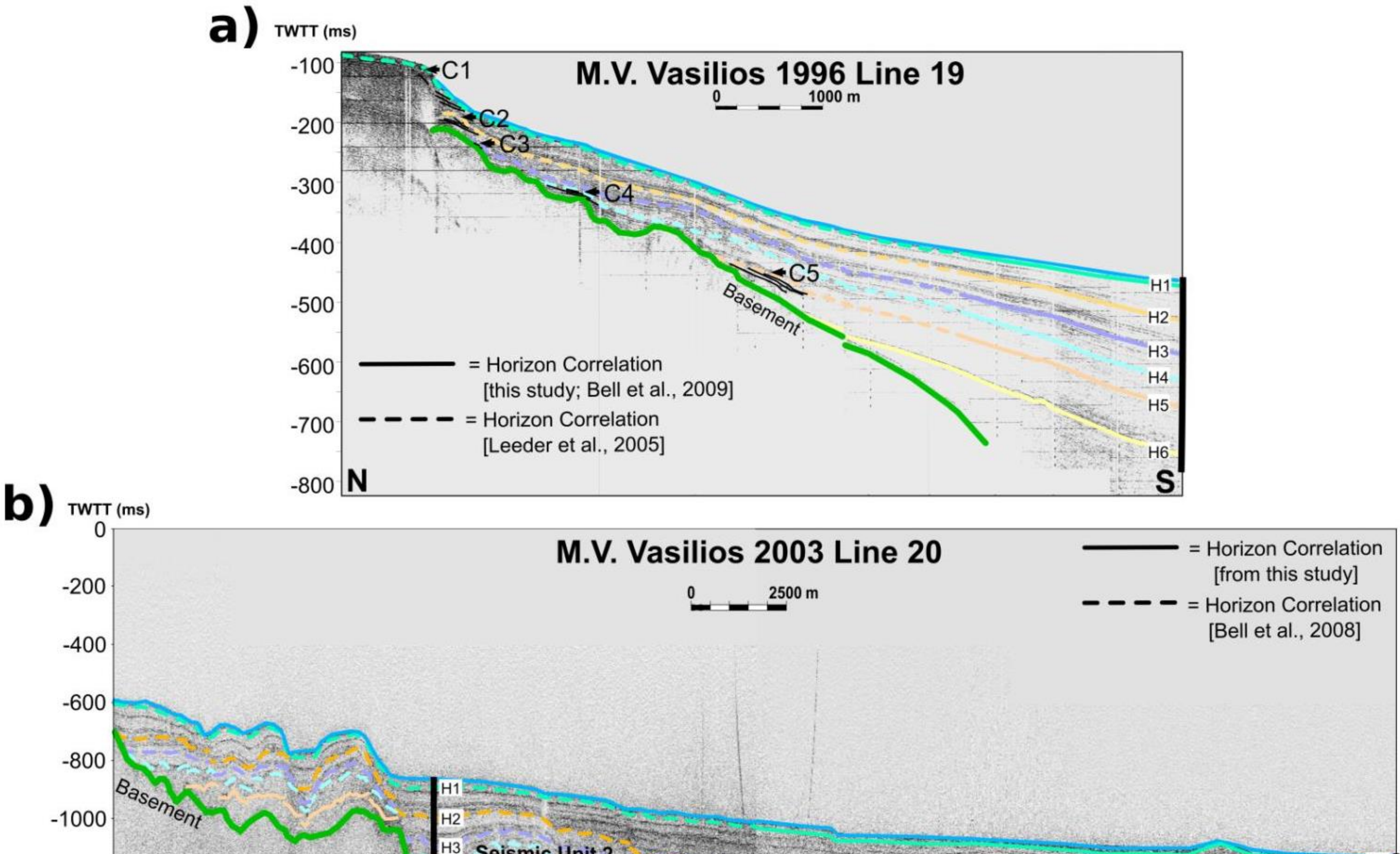
a)
TWTT (ms)
M.V. Vasilios 1996 Line 19
0
1000 m
-100
-200
-300
-400
-500
-600
-700
-800
C1
C2
C3
C4
C5
Basement
= Horizon Correlation
[this study; Bell et al., 2009]
= Horizon Correlation
[Leeder et al., 2005]
H1
H2
H3
H4
H5
H6
N
S
b)
TWTT (ms)
M.V. Vasilios 2003 Line 20
0
2500 m
= Horizon Correlation
[from this study]
= Horizon Correlation
[Bell et al., 2008]
0
-200
-400
-600
-800
-1000
-1200
-1400
-1600
Basement
H1
H2
H3
H4=U
H5
H6
U
Seismic Unit 2
Seismic Unit 1
W
E

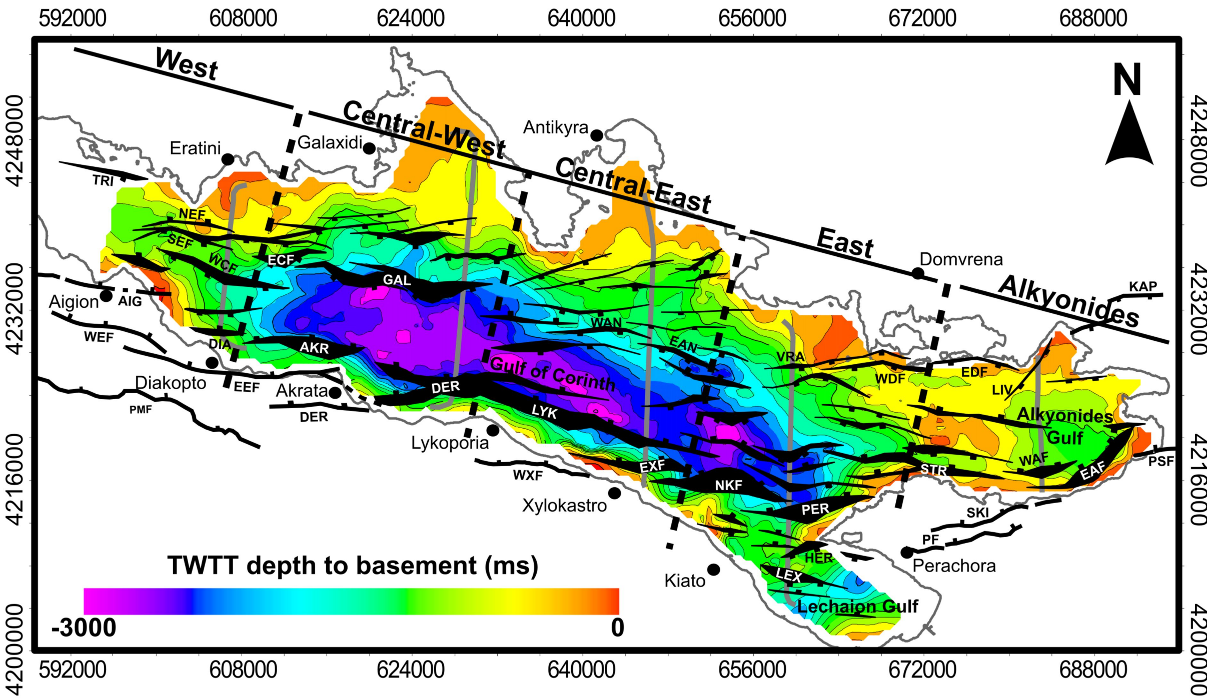

592000
608000
624000
640000
656000
672000
688000
4248000
4232000
4216000
4200000
N
West
Central-West
Central-East
East
Alkyonides
Eratini
Galaxidi
Antikyra
Domvrena
Aigion
Diakopto
Akrata
Lykoporia
Xylokastro
Kiato
Perachora
Gulf of Corinth
Alkyonides Gulf
Lechaion Gulf
TRI
NEF
SEF
WCF
ECF
GAL
AIG
WEF
DIA
AKR
EEF
DER
PMF
LYK
WXF
WAN
EAN
EXF
NKF
PER
HER
LEX
VRA
WDF
EDF
LIV
STR
WAF
EAF
PSF
SKI
PF
KAP
TWTT depth to basement (ms)
-3000
0

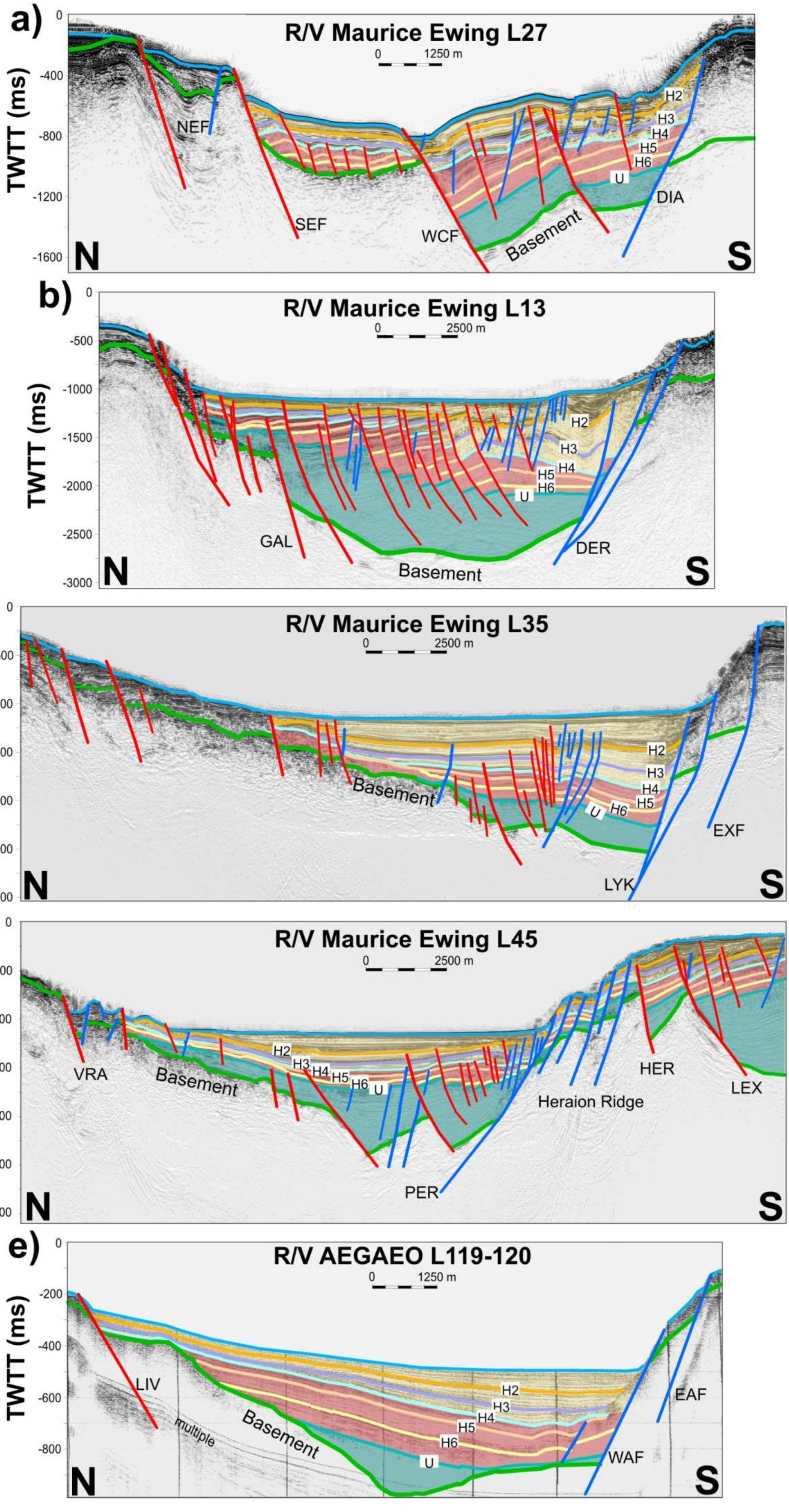

a)
R/V Maurice Ewing L27
0 1250 m
TWTT (ms)
0
-400
-800
-1200
-1600
NEF
SEF
WCF
Basement
DIA
H2
H3
H4
H5
H6
U
N
S
b)
R/V Maurice Ewing L13
0 2500 m
TWTT (ms)
0
-500
-1000
-1500
-2000
-2500
-3000
H2
H3
H4
H5
H6
U
GAL
DER
Basement
N
S
c)
R/V Maurice Ewing L35
0 2500 m
TWTT (ms)
0
-500
-1000
-1500
-2000
-2500
-3000
Basement
H2
H3
H4
H5
H6
U
EXF
LYK
N
S
d)
R/V Maurice Ewing L45
0 2500 m
TWTT (ms)
0
-500
-1000
-1500
-2000
-2500
-3000
H2
H3
H4
H5
H6
U
VRA
Basement
Heraion Ridge
HER
LEX
PER
N
S
e)
R/V AEGAEO L119-120
0 1250 m
TWTT (ms)
0
-200
-400
-600
-800
LIV
multiple
Basement
H2
H3
H4
H5
H6
U
WAF
EAF
N
S

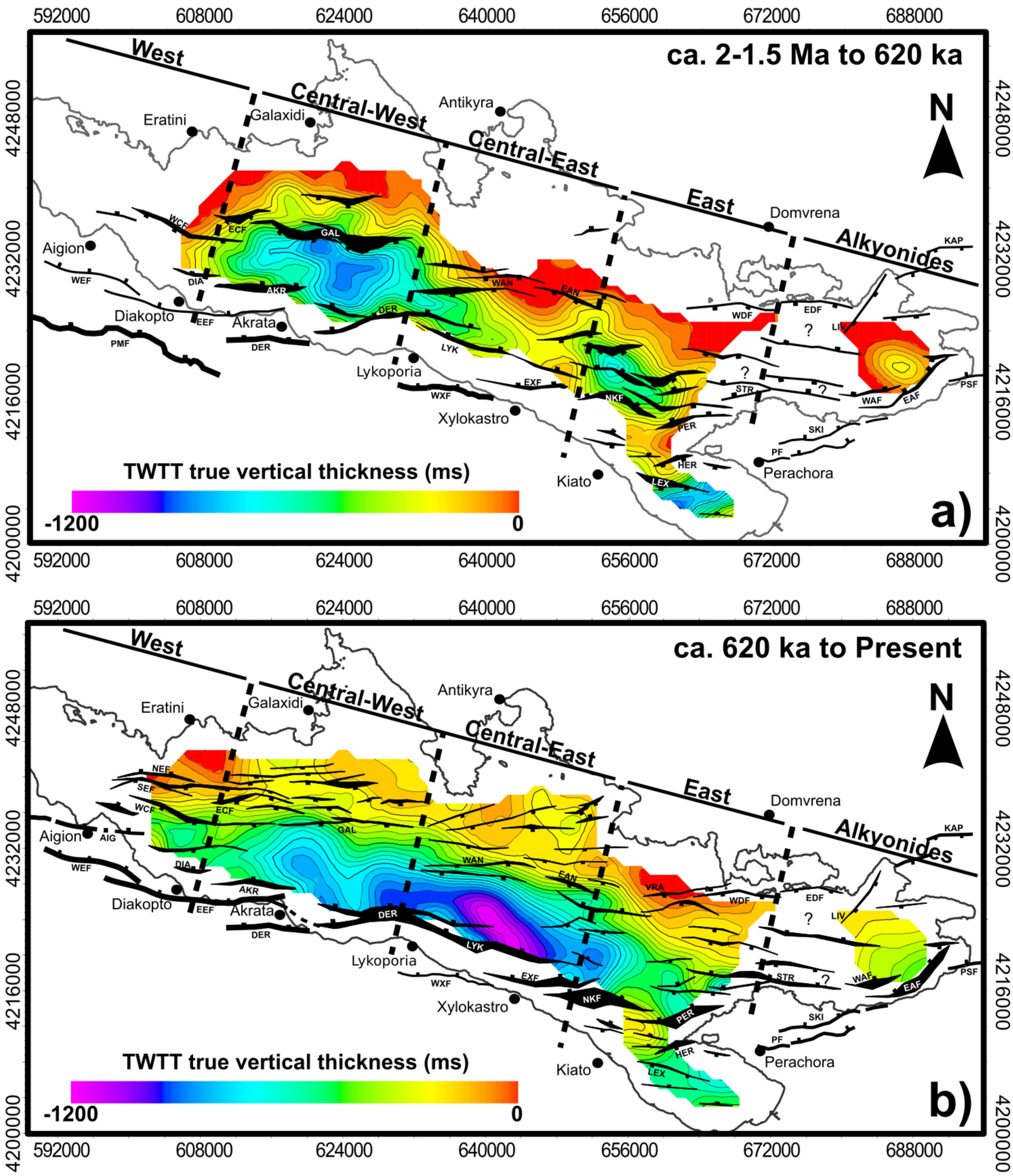

592000
608000
624000
640000
656000
672000
688000
4248000
4232000
4216000
4200000
ca. 2-1.5 Ma to 620 ka
West
Central-West
Central-East
East
Alkyonides
N
Eratini
Galaxidi
Antikyra
Domvrena
Aigion
Diakopto
Akrata
Lykoporia
Xylokastro
Kiato
Perachora
WCF
ECF
GAL
DIA
AKR
DER
WEF
EEF
PMF
WAN
EAN
LYK
EXF
WXF
NKF
PER
HER
LEX
WDF
EDF
LIV
STR
WAF
EAF
PSF
SKI
PF
KAP
?
TWTT true vertical thickness (ms)
-1200
0
a)
ca. 620 ka to Present
NEF
SEF
AIG
VRA
b)

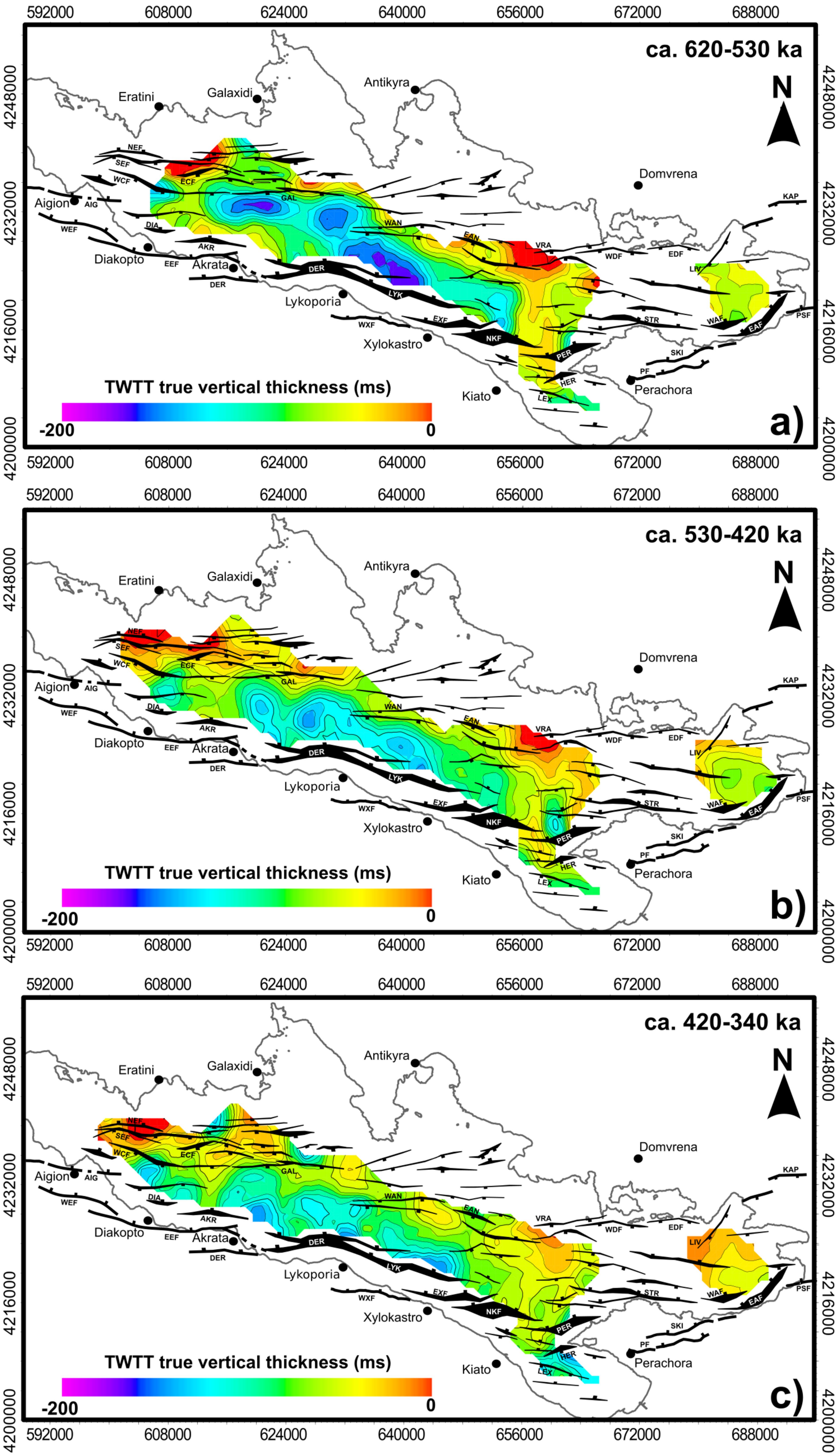
ca. 620-530 ka
N
Eratini
Galaxidi
Antikyra
Domvrena
Aigion
Diakopto
Akrata
Lykoporia
Xylokastro
Kiato
Perachora
NEF
SEF
WCF
ECF
AIG
GAL
WEF
DIA
AKR
EEF
DER
WAN
EAN
VRA
WDF
EDF
LIV
KAP
LYK
EXF
WXF
NKF
PER
HER
LEX
STR
SKI
PF
WAF
EAF
PSF
TWTT true vertical thickness (ms)
-200
0
a)
ca. 530-420 ka
TWTT true vertical thickness (ms)
-200
0
b)
ca. 420-340 ka
TWTT true vertical thickness (ms)
-200
0
c)
592000
608000
624000
640000
656000
672000
688000
4248000
4232000
4216000
4200000

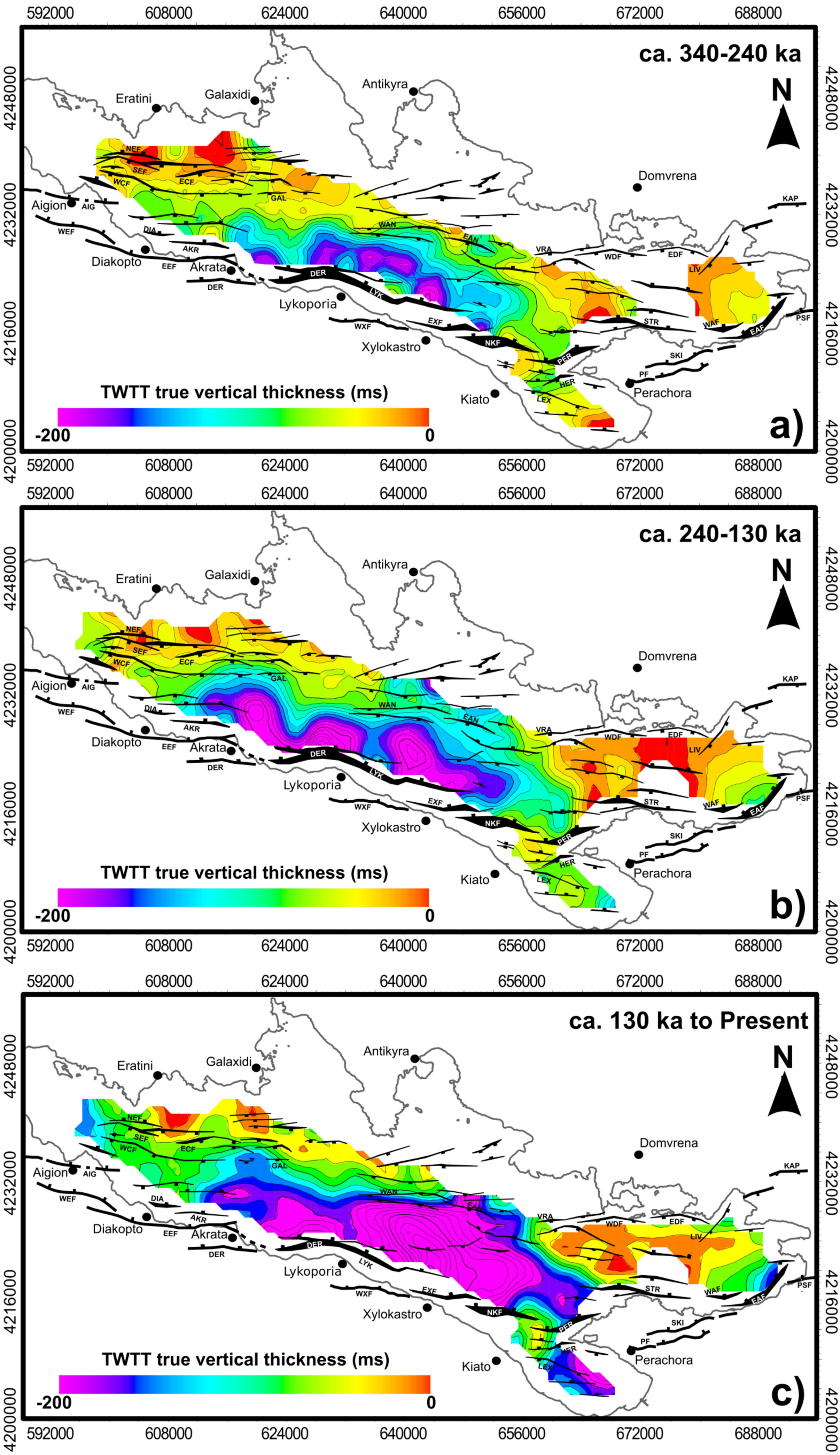

ca. 340-240 ka
ca. 240-130 ka
ca. 130 ka to Present
a)
b)
c)
N
TWTT true vertical thickness (ms)
-200
0
592000
608000
624000
640000
656000
672000
688000
4200000
4216000
4232000
4248000
Eratini
Galaxidi
Antikyra
Domvrena
Aigion
Diakopto
Akrata
Lykoporia
Xylokastro
Kiato
Perachora
NEF
SEF
WCF
ECF
GAL
WAN
EAN
VRA
WDF
EDF
LIV
KAP
AIG
WEF
DIA
AKR
EEF
DER
LYK
WXF
EXF
NKF
PER
HER
LEX
STR
WAF
EAF
PSF
SKI
PF

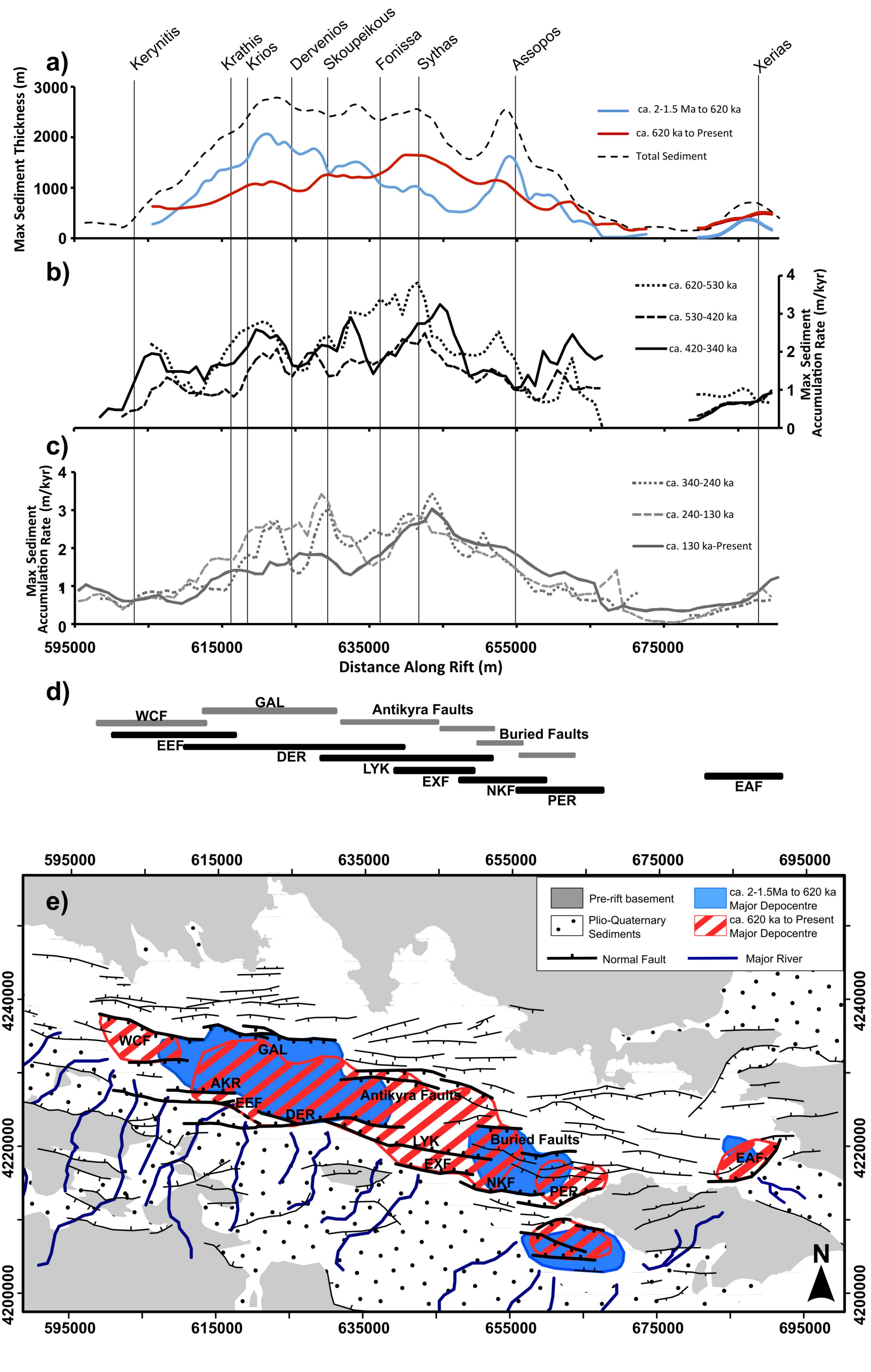
a)
Kerynitis
Krathis
Krios
Dervenios
Skoupeikous
Fonissa
Sythas
Assopos
Xerias
Max Sediment Thickness (m)
ca. 2-1.5 Ma to 620 ka
ca. 620 ka to Present
Total Sediment
b)
ca. 620-530 ka
ca. 530-420 ka
ca. 420-340 ka
Max Sediment Accumulation Rate (m/kyr)
c)
ca. 340-240 ka
ca. 240-130 ka
ca. 130 ka-Present
Max Sediment Accumulation Rate (m/kyr)
Distance Along Rift (m)
d)
WCF
GAL
Antikyra Faults
Buried Faults
EEF
DER
LYK
EXF
NKF
PER
EAF
e)
Pre-rift basement
Plio-Quaternary Sediments
ca. 2-1.5Ma to 620 ka Major Depocentre
ca. 620 ka to Present Major Depocentre
Normal Fault
Major River
AKR
N

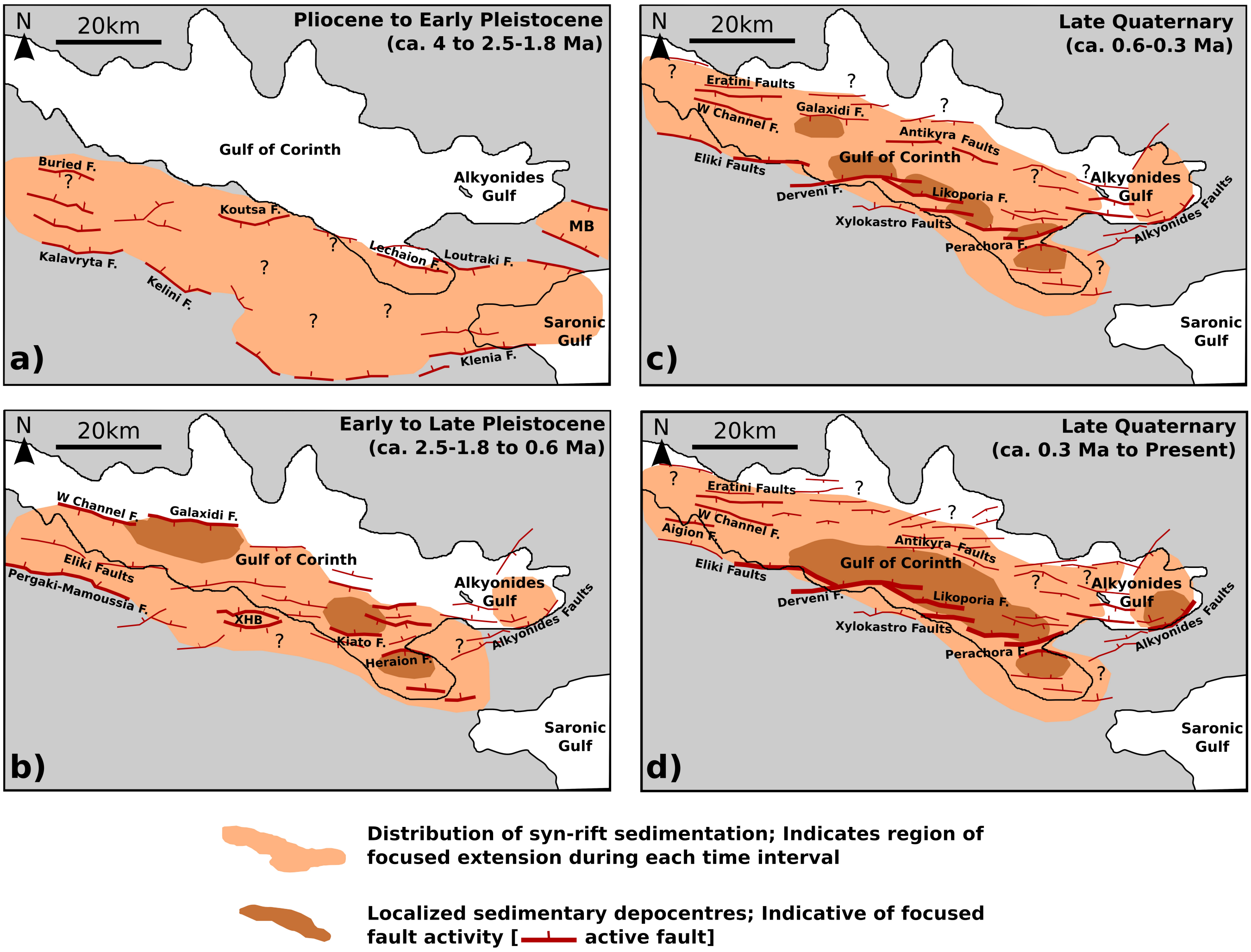
N
20km
Pliocene to Early Pleistocene
(ca. 4 to 2.5-1.8 Ma)
Gulf of Corinth
Alkyonides
Gulf
Buried F.
Koutsa F.
MB
Lechaion F.
Loutraki F.
Kalavryta F.
Kelini F.
Saronic
Gulf
Klenia F.
a)
N
20km
Late Quaternary
(ca. 0.6-0.3 Ma)
Eratini Faults
Galaxidi F.
W Channel F.
Antikyra Faults
Eliki Faults
Gulf of Corinth
Alkyonides
Gulf
Derveni F.
Likoporia F.
Alkyonides Faults
Xylokastro Faults
Perachora F.
Saronic
Gulf
c)
N
20km
Early to Late Pleistocene
(ca. 2.5-1.8 to 0.6 Ma)
W Channel F.
Galaxidi F.
Gulf of Corinth
Eliki Faults
Pergaki-Mamoussia F.
XHB
Alkyonides
Gulf
Alkyonides Faults
Kiato F.
Heraion F.
Saronic
Gulf
b)
N
20km
Late Quaternary
(ca. 0.3 Ma to Present)
Eratini Faults
W Channel F.
Aigion F.
Antikyra Faults
Eliki Faults
Gulf of Corinth
Alkyonides
Gulf
Derveni F.
Likoporia F.
Alkyonides Faults
Xylokastro Faults
Perachora F.
Saronic
Gulf
d)
Distribution of syn-rift sedimentation; Indicates region of focused extension during each time interval
Localized sedimentary depocentres; Indicative of focused fault activity [active fault]

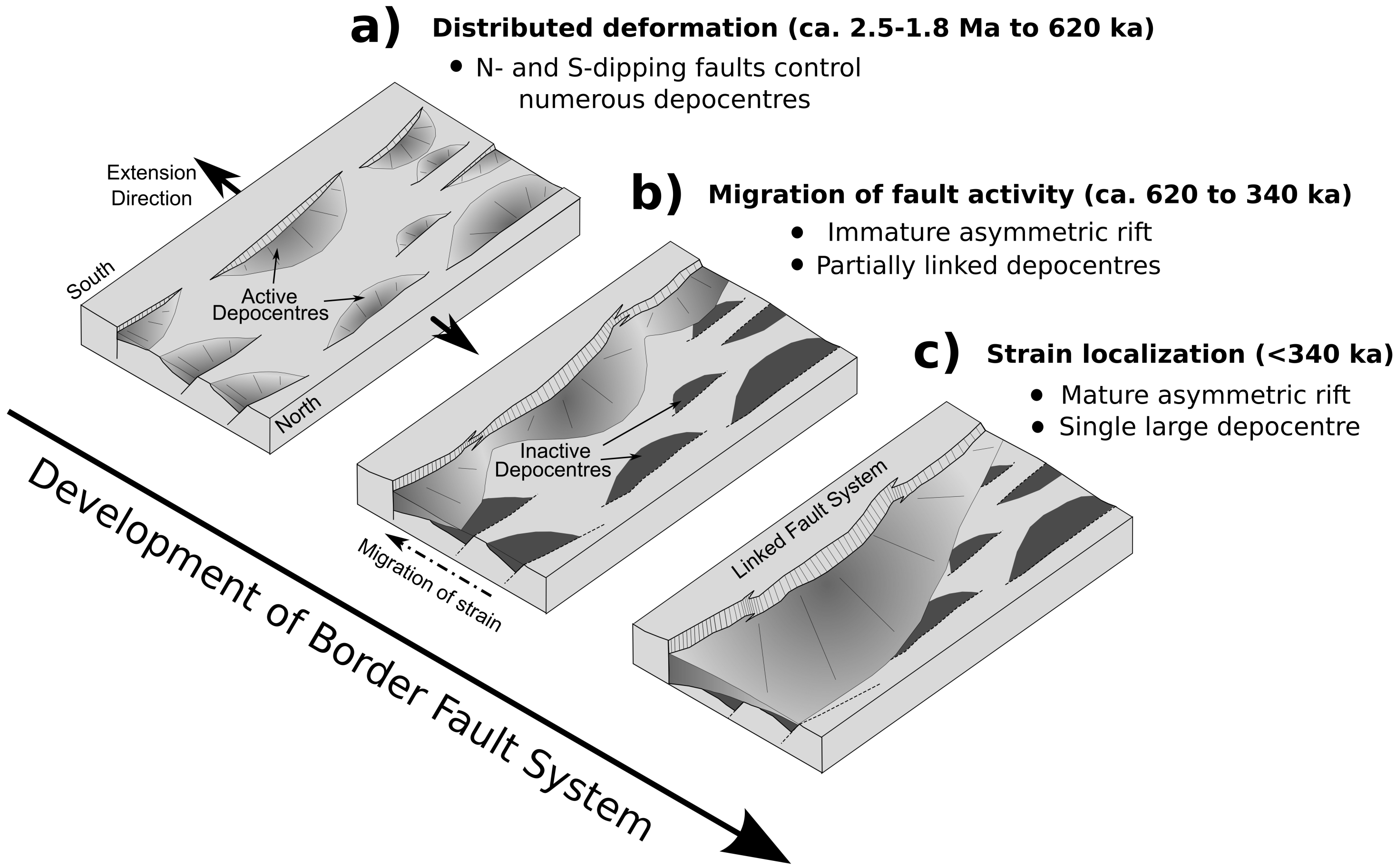
a) Distributed deformation (ca. 2.5-1.8 Ma to 620 ka)
• N- and S-dipping faults control numerous depocentres
Extension Direction
South
North
Active Depocentres
b) Migration of fault activity (ca. 620 to 340 ka)
• Immature asymmetric rift
• Partially linked depocentres
Inactive Depocentres
Migration of strain
c) Strain localization (<340 ka)
• Mature asymmetric rift
• Single large depocentre
Linked Fault System
Development of Border Fault System

Tables

Table 1. Comparison of previous chronostratigraphic models calculated for the offshore Corinth rift.

Study	Region	Method	Identified Glacio-Eustatic Cycles	Unconformity Age Estimate
This Study	**Entire Rift**	**Seismic Character and Clinoforms**	**6 x 100 kyr**	**~620 ka**
Sachpazi et al., 2003	Central Gulf of Corinth	Seismic Character	5 x 100 kyr	~500-600 ka
Bell et al., 2008	Eratini Basin	Clinoforms	4 x 100 kyr	~400 ka
Bell et al., 2008, 2009	Western Gulf of Corinth	Seismic Character	4 x 100 kyr	~300-400 ka
Taylor et al., 2011	Central Gulf of Corinth	Seismic Character	7 x 100 kyr	~680 ka
Leeder et al., 2005	Alkyonides Gulf	Clinoforms	5 x 100 kyr	~500 ka
Sakallariou et al., 2007	Alkyonides Gulf	Seismic Character	4 x 100 kyr	~400-450 ka
Bell et al., 2009	Alkyonides Gulf	Seismic Character & Clinoforms	6 x 100 kyr	~600 ka

Table 2. Summary of rift geometry development for domains shown in figures 5 and 6. See Figure 5 caption for fault nomenclature.

		West	Central-West	Central-East	East	Alkyonides
	Net Geometry	**Symetrical Graben**	**Symetrical Graben**	**S-thickening half-graben**	**S-thickening half-graben**	**S-thickening half-graben**
~340-Present	Rift Geometry	Symetrical	S-thickening	S-thickening	S-thickening	S-thickening
	Controlling Faults	WCF, EEF	DER	LYK, XYL	NKF, PER	EAF
~620-340kyr	Rift Geometry	Slightly N-thickening	Symetrical	S-thickening	Slightly S-thickening	Symetrical
	Controlling Faults	WCF,EEF	GAL, DER	LYK, XYL	NKF, PER	EAF, LIV
~1.5Ma-620kyr	Rift Geometry	Slightly N-thickening	N-thickening	Very little sediment	Numerous N-thickening half-grabens	Symetrical
	Controlling Faults	WCF, EEF, PMF	GAL	-	HER, LEX, Buried faults	EAF, LIV

Table 3. Comparison of the assigned age estimates for boundaries within the onshore and offshore stratigraphic models. See text for discussion.

Onshore Stratigraphic Model			Offshore Stratigraphic Model	
Strat. Group	**Age Est.**	**Study**	**Strat. Unit**	**Age Est.**
----------------	ca. 4-3.6 Ma	Rohais et al., 2007	----------------	
Lower Group			???	
----------------	ca. 2.5-1.8 Ma	Leeder et al., 2012; Ford et al., 2013	----------------	ca. 2-1.5 Ma
Middle Group			Seismic Unit 1	
----------------	ca. 0.7-0.45 Ma	Ford et al., 2013; Rohais et al., 2007	----------------	ca. 0.6 Ma
Upper Group			Seismic Unit 2	
----------------	Present Day		----------------	Present day